SEVENTH FRAMEWORK PROGRAMME
Capacities Specific Programme
Research Infrastructures

Project No.: 227887

SERIES
SEISMIC ENGINEERING RESEARCH INFRASTRUCTURES FOR EUROPEAN SYNERGIES

Workpackage 14
Deliverable 14.3 – Report on centrifuge test techniques with Soil Structure Interaction

Deliverable/Task Leader: UCAM / IFSTTAR
Revision: Final

February, 2012

ACKNOWLEDGMENTS

The research leading to these results has received funding from the European Community's Seventh Framework Programme [FP7/2007-2013] under grant agreement n° 227887.

DELIVERABLE CONTRIBUTORS

UCAM	Charles Heron
	Ulas Cilingir
	Stuart Haigh
	Gopal Madabhushi
IFSTTAR	Sandra Escoffier
	Jean-Louis Chazelas

CONTENTS

Introduction

Soil-structure interaction plays an important role in the dynamic response of many types of structures. In the SERIES project the dynamic soil structure interaction is investigated for a single degree of freedom structure. This is an interesting problem where the dynamic response of the structure combines with the lifting-off of the base during rocking vibrations. Two types of single degree of freedom structures were considered, one with a lumped mass at the top and the other with a sway-frame.

Several centrifuge tests were carried out changing the structures and soil densities. Again there was some overlap between the test specifications. The structures tested at UCAM had bearing pressures of 50 kPa and 100 kPa, while those tested at IFSTTAR had 100 kPa and 300 kPa. Similarly the stiffness of structure was changed in different centrifuge tests. The construction of the model structures was matched as closely as possible between the two centres.

The dynamic response of the structures subjected to model earthquake loading was measured in several different ways. Some techniques of measurement were common between UCAM and IFSTTAR, while others such as advanced dynamic PIV measurements based on fast digital imaging were carried out at UCAM only. This technique is able give the soil displacement vectors at different points within an earthquake loading cycle. In all centrifuge tests, the accelerations within the soil and at different locations on the structure were measured using miniature accelerometers. The acceleration data was used to obtain the moment-rotation loops for the structure for different earthquakes. These were compared for structures of different stiffness, foundation soil placed at different relative densities and earthquakes of different intensity and frequency content.

In this report details are given of the general theory of centrifuge modelling. This is followed by the experimental facilities, centrifuge model containers, instrumentation and data acquisition used at UCAM and IFSTTAR facilities. The details of the design of different model structures are also presented. Following this, the model preparation techniques including the air-pluviation devices used are presented. The technique of PIV analysis using digital images from a fast digital camera is introduced. Following this the experimental data obtained in each centrifuge test such as acceleration time histories, settlement time histories and the results of the analyses of the data in the form of moment-rotation loops are presented. Results from some of the selected PIV analysis are also shown. Finally a brief summary of the research carried out in JRA 3.2 work package and the main outcomes are presented.

Centrifuge Modelling Theory

Centrifuge modelling has become popular among geotechnical researchers since the 1960s as an effective way to test small scale geotechnical models while still being able to obtain quantifiable results applicable to full scale scenarios.

Small scale soil models tested at 1-g will be at a stress state significantly lower than that present in the prototype scenario being modelled. Hence, with soil having non-linear stress-strain behaviour, tests conducted at 1-g cannot provide quantifiable results relating to the prototype scenario. Full scale models are far too costly and time consuming to construct and hence, when an accurate model of a geotechnical situation is required centrifuge modelling is utilised.

When models are tested in a geotechnical centrifuge a ‘g-level’ (N) will be chosen which defines the level of centrifugal acceleration which the model will be subjected to. However, due to centrifugal acceleration being proportional to radius ($a_c = r\omega^2$), the g-level will increase with depth through the model. In addition, the centrifugal acceleration will be constant along a circular path of constant radius; hence a rectangular model will not have a constant g-level at one depth. To minimise the impact of these effects on the results obtained geotechnical centrifuges are generally quite large so the height of the model is small compared to the overall radius of the centrifuge. In addition, a g-level is chosen that minimises the overall error in the stress distribution compared to the prototype, this is often referred to as the ‘nominal g-level’. In certain situations, for example when calculating the precise bearing pressure of a shallow foundation located on a sand deposit, the average g-level experienced over the height of the model structure will be used instead of the nominal g-level.

A set of scaling laws have been derived and validated to covert between prototype and model scales using the conversion factor of the g-level (N). The laws were presented by Schofield 1980 & Schofield 1981 and are summarised in Table 1.

Table 1: Summary of Centrifuge Scaling Laws

Parameter	**Model / Prototype**	**Dimensions**
Length	$1 / N$	L
Mass	$1 / N^3$	M
Stress	1	$ML^{-1}T^{-2}$
Strain	1	1
Force	$1 / N^2$	MLT^{-2}
Seepage Velocity	N	LT^{-1}
Time (Seepage)	$1 / N^2$	T
Time (Dynamic)	$1 / N$	T
Frequency	N	T^{-1}
Acceleration	N	LT^{-2}
Velocity	1	LT^{-1}

after Schofield (1980, 1981)

Experimental Equipment - UCAM

Centrifuge

At UCAM the 10m Turner Beam Centrifuge was used to conduct this series of tests. The tests described in this report were all conducted at 106rpm which corresponds to 42g at the level of the structures and a nominal g-level of 46g. The Turner Beam centrifuge has two arms of equal length - nominally 4.125 metres; one end supports the model, the other carries a counterweight mass as pictured in Figure 1. The machine has a capacity of 140g-ton with a maximum centrifugal acceleration of 120g. However, for dynamic models the maximum allowable g-level is approximately 50g due to the constraints of the SAM actuator which is discussed below. More details on the centrifuge can be found in Schofield 1980.

Figure 1: 10m Turner Beam Centrifuge

Shaker

To induce earthquake motions in the models the Stored Angular Momentum (SAM) actuator at UCAM was used. The SAM actuator works by spinning two flywheels up to the required speed. A clutch mechanism then grabs hold of a reciprocating rod coming from the flywheels which transmits shaking into the model until the clutch releases. A view of the SAM actuator and a schematic diagram showing the principle of its operation are presented in Figure 2. The duration, frequency and magnitude of the earthquake can be set independently while the centrifuge is spinning. The system is very simple and very reliable. However, it is capable of inducing only two types of earthquake: a single frequency, single amplitude earthquake or an earthquake of decreasing magnitude, decreasing frequency (sine-sweep). An example trace of both these types of earthquake is shown in Figure 3. For this series of tests these earthquake motions were more than ample to produce data suitable for making the conclusions found later in this report. More information on the SAM actuator can be found in Madabhushi *et al.* 1998.

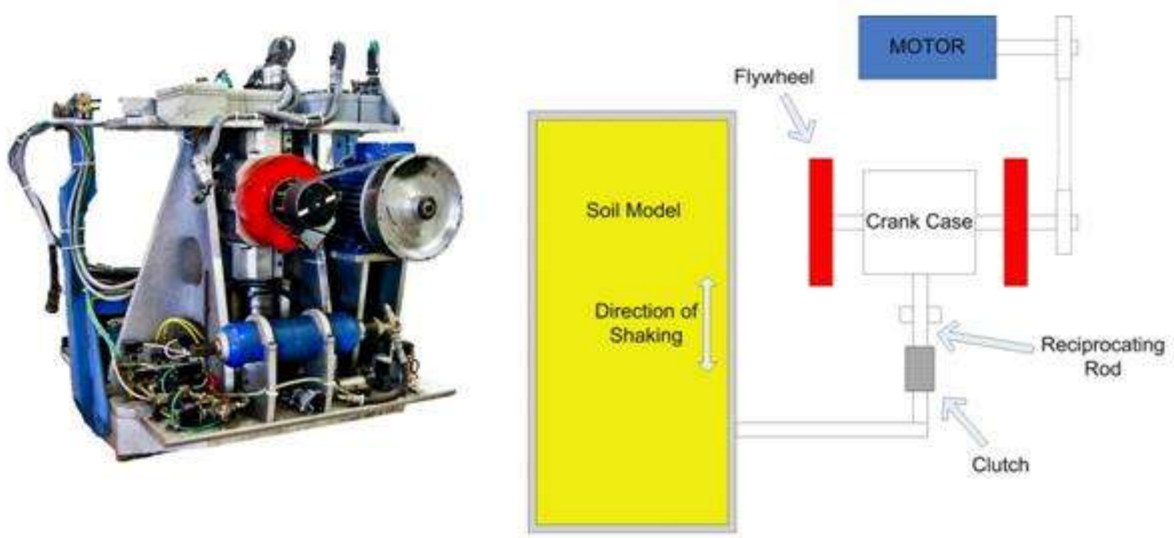

Figure 2: SAM Earthquake Actuator

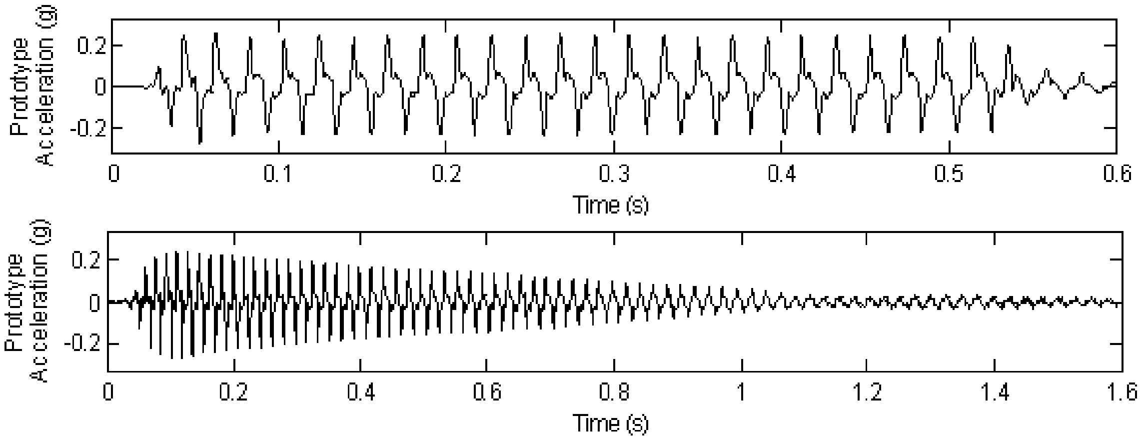

Figure 3 – Example Earthquake Traces from SAM Actuator
Top: Simple Sinusoidal Earthquake – constant magnitude & constant frequency
Bottom: Sine-sweep Earthquake – decreasing magnitude & decreasing frequency

Model Container

Equivalent Shear Beam (ESB) Box

Unlike for static centrifuge tests, a rigid model container is not ideal for use in dynamic centrifuge models as the rigid boundaries of the container will affect the response of the soil contained within the box. Instead, for the first set tests an Equivalent Shear Beam (ESB) Box was used. The ESB box consists of aluminium rings connected and separated with layers of rubber. The stiffness of the ESB box used in this series of tests is designed to match the natural frequency of a sand column with a voids ratio of 0.77 (58% relative density for Hostun sand) at 50g. This means that the boundaries fundamentally act the same as the sand during dynamic loading. As relative density has a minimal impact on the natural frequency of the soil column, models can be tested at different relative densities without any significant impact from the boundaries. A view of the ESB model container is shown in Figure 4. More details on the ESB box design and construction can be found in Brennan and Madabhushi, 2002.

Figure 4: ESB (flexible) Model Container

Window Box

For the tests utilising PIV (see Section on PIV analysis), a box with a transparent side was required to allow the soil movements to be photographed during the shaking. Due to the technical difficulties in constructing a flexible box like the ESB box with a transparent side, a rigid box has to be used for the PIV tests. The rigid window box has three metal sides and one transparent Perspex wall as shown in Figure 5. To minimise the effect of the rigid boundaries on the response of the sand within, duxseal (a plumbers material typically used for sealing pipes) is added to either end wall. The duxseal acts to absorb the energy of the waves as they enter it and hence it reduces the amount of energy reflected back into the sand body. It has been experimentally verified that the duxseal reduces the magnitude of the wave reflections sufficiently such that they will not have an impact on the response monitored, Steedman and Madabhushi, 1991. More details on the Window Box can be found in Cilingir and Madabhushi, 2011.

Figure 5: Window (rigid) PIV Model Container

Instrumentation

Piezoelectric Accelerometer

Piezoelectric accelerometers are the traditional transducer used to measure acceleration in dynamic centrifuge experiments. When they are subjected to vibration, a crystal within the instrument gets squeezed which in turns releases a charge. This charge output is converted into a voltage using a charge amplifier. These instruments have a natural inbuilt high pass filter meaning they are ineffective at measuring accelerations at low frequency (approximately below 5 Hz). However, the frequencies being measured in this series of tests are well within the useable range of the piezoelectric accelerometers.

Figure 6: Piezoelectric Accelerometer

Micro-electro-mechanical System Accelerometer

Micro-electro-mechanical System (MEMS) accelerometers are small electrical devices which measure acceleration by measuring the force a mass applies to a spring. This means that they also measure inertial acceleration as well as dynamic acceleration. They have been used widely in geotechnics for field monitoring and have been used in 1g testing. More recently their use in dynamic centrifuge tests has been investigated due to their small size, small weight and significantly lower cost compared to their piezoelectric counterparts. As part of this project (JRA 2) the use of MEMS accelerometers has been investigated by combining their use with traditional piezoelectric accelerometers in the models and comparing the resulting signal quality, Stringer *et al* 2010. In the series of tests discussed in this report, MEMS were primarily utilised to monitor the response of the model structure. An example of one of the MEMS accelerometer used in this project is shown in Figure 7.

Figure 7: MEMS Accelerometer

Linear Variable Differential Transformer (LVDT)

During Phase I testing, to measure the vertical location of the structures and the level of the free-field sand surface pre and post each earthquake, Linear Variable Differential Transformers (LVDTs) were utilised. A view of the LVDT is presented in Figure 8. These devices have a relatively slow response time meaning they are ineffective at measuring high frequency displacements accurately (over ~15Hz). They do however provide an accurate indication of the cumulative settlement. It is possible to determine the higher frequency displacement information from the double integral of an appropriate acceleration trace. Combining this with the low frequency displacement component measured by the LVDT, it is theoretically possible to determine the full displacement trace during dynamic loading.

Figure 8: LVDT Displacement Transducer

Air hammer

To allow a comparative numerical analysis to be conducted, knowledge about the stiffness of the sand within the models is required. To achieve this, an air hammer was installed at the bottom of each model during the Phase I testing. Through a set of valves, air is supplied to one end of the air hammer which pushes a metal pellet within the air hammer causing it to impact on the opposite end of the air hammer. This induces a shear wave in the model. A view of the air hammer is shown in Figure 9. The speed at which the shear wave moves up through the model can be determined through measurement using piezoelectric accelerometers. To determine the small strain stiffness, as low an air pressure as possible was used in order to induce as small a strain as possible within the model.

Figure 9: Air hammer for inducing shear waves in model

High Seed Camera

Due to the scaling laws discussed earlier, earthquakes in the centrifuge last only about 0.5 seconds at a frequency of about 50 Hz. Therefore to capture images a high speed camera is required. For this series of tests a MotionBLITZ EoSens® mini2 camera was used which is capable of recording images at a 3 Megapixel resolution at up to 523 frames per second. Due to certain parts of the field of view not being of interest in these tests the image size was reduced to only look at the relevant parts. This allowed the frequency of image recording to increase up to 1000 frames per second. The camera body measures 65x65x65mm and a c-mount lens with a fixed focal length of 12.5mm was used as shown in Figure 10. Due to the short exposure times requires (to eliminate blur in the images) high power LED lights (100W each) were used to illuminate the model.

Figure 10: High Speed Camera with Lens

Data Acquisition

The UCAM earthquake data presented in this report was acquired through the 'Centrifuge Data Acquisition System' (CQADS), which was developed by Carrack in partnership with the geotechnical group at Cambridge University. This system allows up to 32 channels to be sampled at up to 4 kHz. This system is used in preference to DASYLab or LabVIEW as it stores the data locally until after the earthquake. The short path from instrument to signal digitisation allows the signal noise to be minimised. Signal noise is a particular problem on the SAM actuator due to the motors required to drive the flywheels.

Due to the limited acquisition speed of CDAQS, a separate accelerometer array was installed in the models to detect the air hammer shear wave progression. These accelerometers were monitored using DASYLab as the air hammer was not fired during the earthquake and hence noise interference with the signal from the motor on the SAM was not an issue. A sampling rate of 50 kHz was used while monitoring the piezoelectric accelerometers during air hammer tests.

Experimental Equipment – IFSTTAR

Centrifuge

The IFSTTAR Centrifuge is a beam centrifuge with a radius of 5,50 m and a capacity of 200 t-g in operation since 1985. In the configuration of an additional device – the earthquake simulator - is settled in the basket. A view of the centrifuge is presented in Figure 11.

Figure 11 General view of the IFSTTAR Centrifuge

Shaker

The earthquake simulator at the IFSTTAR is an electro-hydraulic system developed by Actidyn System (see figure 12). Its physical characteristics are given in Table 2.

Figure 12: General view of the QS80 Earthquake Simulator at IFSTTAR

The shaking table generates a horizontal acceleration time sequence at the bottom of the box. Horizontal means perpendicular to the centrifuge accelerations which substitutes to the natural vertical gravity acceleration. It is named at the Y direction, the vertical of the model being Z and the X direction being tangential to the rotation circle. At IFSTTAR the Y direction is vertical when the basket is tilted.

For those who are not used to centrifuge test, it should be recalled that the controlled earthquake sequence is that obtained on the shaking table and applied at the bottom of the sand layer.

The two main characteristics of IFSTTAR earthquake simulator as regard to that at UCAM are:

- the ability to perform both sine inputs and “real earthquake inputs”
- the fact that the driving functions (the electrical signal) applied to the servo-valves to obtain the target acceleration sequence on the shaking table is tuned preliminary to the tests series on a dummy sand box (with similar mass and stiffness characteristics as the test payload). Once the target acceleration sequence obtained on the dummy payload, the same driving function is applied to every the sand box prepared for the experimental program. This should, normally, warrant that the input at the bottom of the box is constant.

Table 2: Characteristics of the IFSTTAR shaker

Shaking platform length	1	m
Shaking platform width	0.5	m
Payload height	0.6	m
Payload Mass (including box)	400	kg
Centrifuge acceleration of operation	200 to 800	m/s/s
Maximum displacement	5	mm
Maximum velocity.	1	m/s
Maximum acceleration	400	m/s/s
Frequency range (for earthquake inputs)	20 à 300	Hz
Frequency range (for sine inputs)	20 à 200	Hz

Model container

IFSTTAR container used for this series of tests is a Flexible Shear Beam model developed in 2008. It is made of 14 identical frames of aluminium frame large by 2,5 cm height piled with 4 mm rubber sheets in between frames (Figure 13). An internal report prepared by Escoffier (2008), tests of this box on a shaking table show a resonance between 32 and 37 Hz.

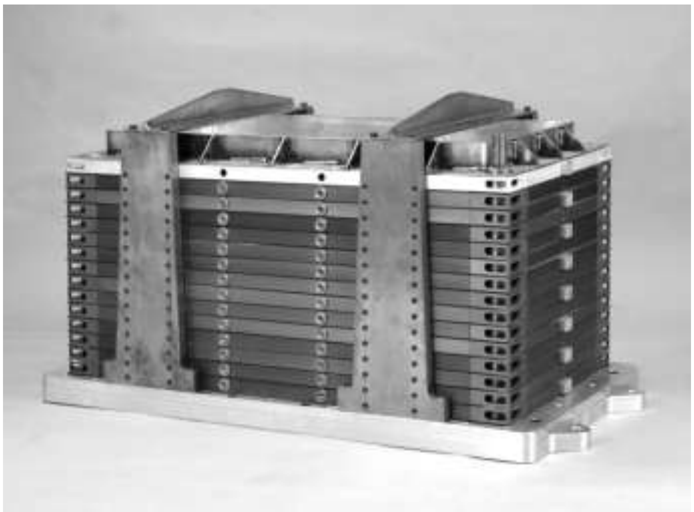

Figure 13: A view of the IFSTTAR ESB Box (note that the top ring made of steel sheets is only made for the pluviation process and is removed in operation)

Instrumentation

Piezoelectric Accelerometer

The Piezoelectric accelerometers used by the IFSTTAR are Brüel & Kjaer type 4517 shown in Figure 14. Their small weight (0.6g) avoids the effect of the sensors on the measurement. They have a natural inbuilt pass band filter of 1Hz to 20kHz. It means that a double integration process applied on the measuring data will only enable to obtain the dynamic displacement (and not the residual one). It should be noticed that concerning the high cut off frequency is largely higher than all the interesting frequencies for the centrifuge tests.

Figure 14: Piezoelectric Accelerometer

Laser sensors

Two type of laser sensors have been used the JRA3 tests. Low frequency laser sensors have been used for the measurement of the soil and the building settlement. They have a cut off frequency of 100 Hz. For the recording of the building movement during the seismic event fast response laser sensors with a frequency range from 0 up to 10 kHz have been used. A view of the laser sensors is shown in Figure 15. These sensors enable us to follow the building movement during the seismic event considering that a correction should be made due to their own movement during the seismic event.

Figure 15: High frequency laser sensor

Fast data acquisition system

The fast data acquisition system at IFSTTAR is an LMS system. This system allows us to acquire 72 channels of data with a synchronized acquisition. The data acquisition system is located in the basket and data are transmitted through slip rings in the pivot to the command room. The time delay for the data transmission is negligible. Figure 16 illustrate this fast data acquisition system.

Figure 16: Fast data acquisition system

It must be pointed out that the soil and building settlement are recorded with the low frequency data acquisition system that is composed of SPIDER system.

Design of Model Structures

Phase I Structures

During seismic loading the dominant shaking frequency is often in the region of 1-2 Hz which matches the natural frequency of many buildings that have approximately 5 storeys, making such buildings very vulnerable to damage during earthquakes. Therefore, a 5 storey building, with a natural frequency of 1 Hz situated on shallow raft foundation is the prototype that will be investigated in this series of tests. It is not feasible to scale down every detail of the real building. Hence, certain key parameters were chosen which were considered to have the largest influence on the response of the soil-structure interface. These included; bearing pressure, natural frequency, superstructure to foundation mass ratio and aspect (height to width) ratio.

Initially, two simple lumped mass structures were designed and constructed as detailed in Table 3 and shown in Figure 17 – denoted ‘StructA1’ and ‘StructA2’ (Type A structures). However, with these structures it was difficult to tune one parameter without affecting another and hence the structures did not possess the exact properties desired after tuning. This was not a significant problem as these structures were only used for the initial two tests of Phase 1 (CH01 & CH02) which were aimed primarily at examining potential structure-soil-structure interaction.

Figure 17: Type A Structure (example shown is A1 – 50 kPa bearing pressure)

In the case of the tests performed at the IFSTTAR center, 2 structures based on the design of the structure A1 and A2 have been used. They are denoted 'StructA2-bis' and 'StructA3'. The characteristics of these structures are given in Table 3.

For tests CH03 & CH04, new sway frame structures were designed ('Struct B1' & 'Struct B2' – Type B structures). The sway frame structures were chosen as they would result in a less significant rocking mode than the lumped mass structures and hence are believed to represent the prototype more accurately. These were designed in such a way that all the desired properties could be achieved precisely. They are shown in Figure 18.

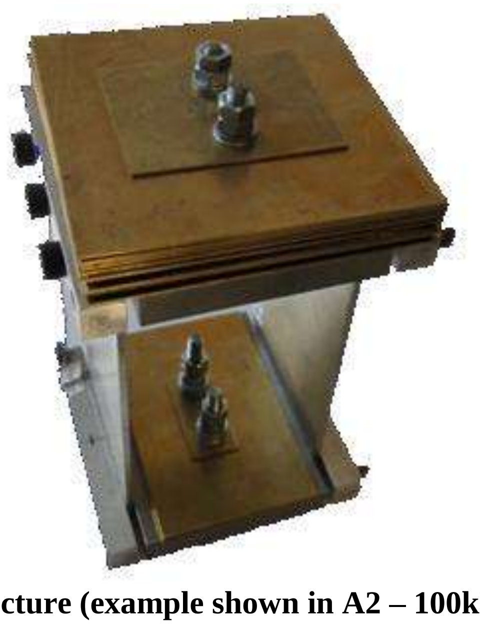

Figure 18: Type B Structure (example shown in A2 – 100kPa bearing pressure)

To tune the structures to the desired parameters, mass was removed and added to the superstructure and foundation of the Type A structures to obtain the correct bearing pressure and natural frequency. Unfortunately this resulted in the incorrect superstructure-foundation mass ratio. The Type B structures were tuned by adjusting the mass of superstructure and foundation to obtain the correct superstructure-foundation mass ratio and bearing pressure. Subsequently the natural frequency was tuned by adjusting the size of the aluminium webs hence allowing all three parameters to be set.

Table 3: Properties of Type A and Type B Structures (prototype scale)

	Struct A1	Struct A2	Struct A2-bis	Struct A3	Struct B1	Struct B2
Nominal Bearing Pressure (kPa)	50	100	100	300	52	98
Fixed Base f_n (Hz)	1.0	1.0	1.0	1.0	1.0	1.0
Centre of Gravity (m)	2.9	2.6			4.4	4.8
Superstructure Mass (tonne)	44	75			61	119
Foundation Mass (tonne)	31	88			20	40
Superstructure : Foundation	1.3	0.9			3.1	3.0
Base Width (m)	4.0	4.0	4.0	4.0	4.0	4.0
Height (m)	6.0	6.0			6.0	6.0
Length (m)	4.0	4.0	4.0	4.0	4.0	4.0
Frame Material	Alumin.	Alumin.	Alumin.	Alumin.	Alumin.	Alumin.
Surcharge Material	Brass	Brass	Brass	Brass	Brass	Brass

PIV Model Structures

There were three different types of structures used for the PIV tests. All of the structures were strip footings instead of isolated pad footings. The structures had to be the full depth of the box as once the centrifuge package adopts the in-flight position the Earth’s gravity field acts in the direction which would pull the model structure away from the Perspex window. Hence, in order to hold the front end of the structure tight against the Perspex screen a sprung ram system (as shown in Figure 19) was used between the back end of the structure and the rear wall of the window box. It is important that as the structure responds to the earthquake it displaces the sand which lies directly against the window, as only that sand will be observed in the images being acquired for the PIV analysis; hence why such care was taken to ensure it remained flush with the Perspex window.

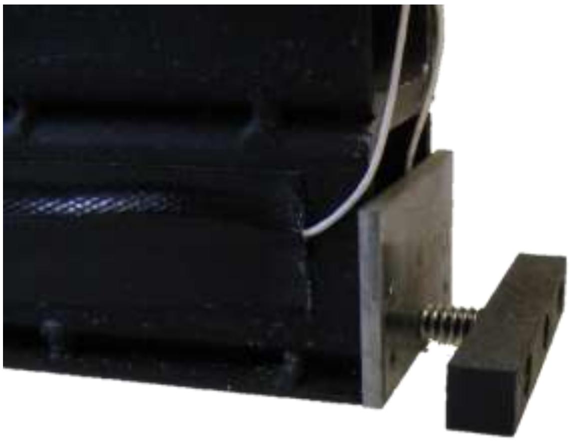

Figure 19: Sprung Support System (attached to Struct D2)

The first structure (Type C) tested (shown in Figure 20) was an aluminium sway frame with brass surcharges added to the superstructure and foundation, similar to the Type B structures. The webs are interchangeable allowing for flexible and stiff versions of the structure to be tested. The dimensions of the Type C structure are identical to the Type B structures except with respect to it being a strip opposed to an isolated pad – this allowed the response of the Type C structure tested in the window box to be compared to the response of the Type B structure tested in the ESB box. The properties of Type C structure are shown in Table 4.

Figure 20: Type C Structure (example shown is C2)

Table 4: Properties of Type C Structures (prototype scale)

	Struct C1	Struct C2
Nominal Bearing Pressure (kPa)	100	100
Fixed Base f_n (Hz)	1	>400
Centre of Gravity (m)	4.5	4.5
Superstructure Mass (tonne)	321	321
Foundation Mass (tonne)	108	108
Superstructure : Foundation	3.0	3.0
Base Width (m)	4.2	4.6
Height (m)	6.0	6.0
Length (m)	10.5	10.5
Frame material	Alumin.	Alumin.
Surcharge Material	Brass	Brass

However, the width of the Type C structure meant that the entire soil deformation mechanism could not be observed within the field of view of the camera. Hence a smaller model structure, made from welded together pieces of steel box section and plate, was constructed as shown in Figure 21. The first version of this structure, Type D1, consisted of only a single piece of box section and did not have a high enough centre of gravity. A second version was therefore built (Type D2, shown in Figure 22) which consisted of two box sections on top of each other. Both Type D1 & D2 could be placed on the sand surface either way up, i.e. modelling a structure either with a high centre of gravity or a low centre of gravity. The structures with a low centre of gravity are of interest when trying to induce sliding in the soil-structure interface. The type D structures have a very high natural frequency due to the inherently stiff nature of the steel box sections. The properties of Type D structure are given in Table 5.

Figure 21: Type D1 Structure (example shown is D1a)

Figure 22: Type D2 Structure

Table 5: Properties of Type D Structures (prototype scale)

	Struct D1a	Struct D1b	Struct D2
Nominal Bearing Pressure (kPa)	100	100	100
Fixed Base f_n (Hz)	>400	>400	>400
Centre of Gravity (m)	1.7	0.9	2.7
Base Width (m)	2.5	2.5	2.5
Height (m)	2.6	2.6	4.6
Length (m)	10.5	10.5	10.7
Frame material	Steel	Steel	Steel
Surcharge Material	Steel	Steel	Steel

The final structure tested was a simple steel bar with no superstructure (Type E shown in Figure 23). It was tested as part of the investigation into sliding as its lack of superstructure mass, and hence very low centre of gravity, should facilitate a sliding mode in preference to a rocking mode. The properties of Type E structure are shown in Table 6.

Figure 23: Type E Structure

Table 6: Properties of Type E Structure (prototype scale)

	Struct E
Nominal Bearing Pressure (kPa)	100
Fixed Base f_n (Hz)	-
Centre of Gravity (m)	0.6
Base Width (m)	2.5
Height (m)	1.3
Length (m)	10.5
Material	Steel

Experimental Procedure-UCAM

Model Preparation

The models were prepared and then loaded onto the centrifuge arm once the entire package was ready to be tested. Dry Hostun sand was used for these tests which was air-pluviated through a robotic sand pourer. Instruments were placed at pre-defined positions during the air-pluviation process. More information on Hostun Sand and the Automatic Sand Pourer can be found below.

Hostun Sand

The sand used in preparing the models tested was HN31 Hostun Sand from France (Flavigny, 1990). The particle size distribution (PSD) is shown in Figure 24. New Hostun sand has a coefficient of uniformity of 1.67 with a d_{50} size of 480 microns.

As the tests were carried out using dry sand, the Hostun sand was reused for several tests. To check that this was not affecting the particle size distribution, a sample was tested again after two tests as shown in Figure 24. The coefficient of uniformity dropped marginally to 1.63 meaning the sand was more uniform and the d_{50} size reduced to 447 microns. It would be expected for the sand to accumulate fines due to crushing of the larger sand grains. However, the variation between these two PSD curves could also be due, in part, to the sand sample for the new Hostun sand PSD curve coming from a different batch to the sand used for the centrifuge tests. The sand used for the centrifuge tests was not tested prior to the first centrifuge test; instead a sample of the current stock (which was from a new delivery) was taken to be tested as `new Hostun'. Currently, it is not known how consistent the PSD curves are between different delivery batches.

Accumulation of fines in the sand would be expected to lead to an increase in stiffness. This is due to the sand grains becoming increasingly difficult to crush and it becoming more difficult for them to move around each other as they get smaller. However, any increase in stiffness resulting from the changes in the PSD curves shown in Figure 24 will be negligible when compared to the variation in stiffness caused by the variation (+/- 5%) in obtaining the correct relative density.

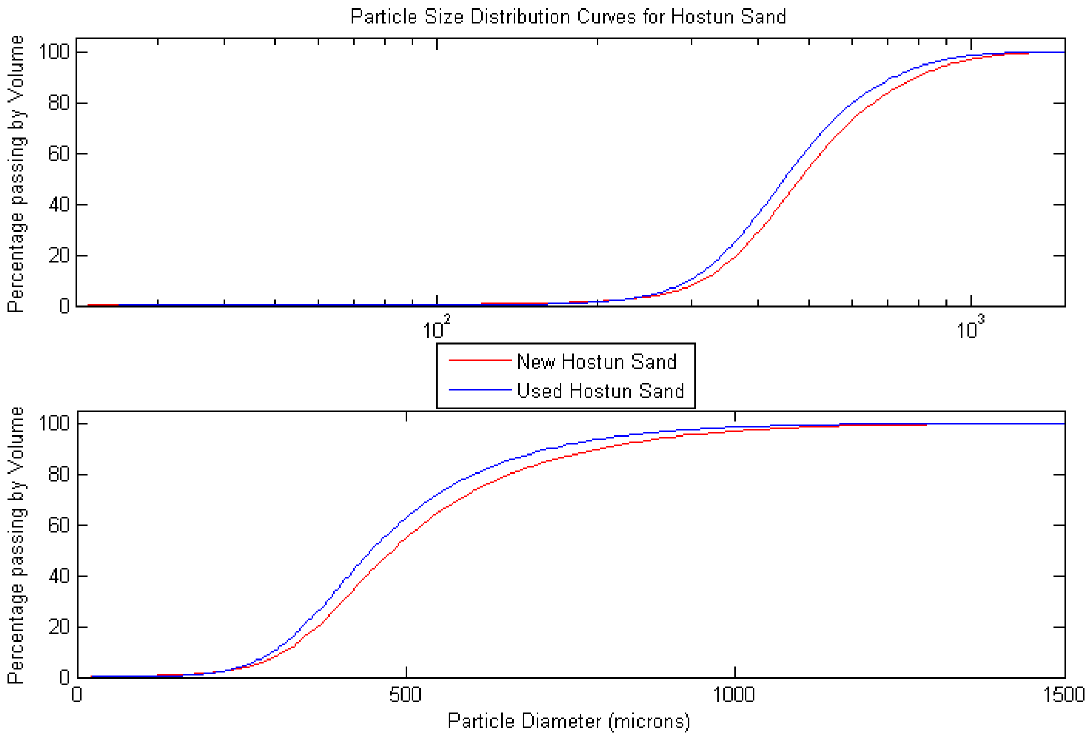

Figure 24: Particle size distribution curves for Hostun Sand

Automatic Sand Pourer

To achieve a specific relative density the sand needs to be poured from a particular height and at a particular flow rate. This was traditionally achieved by using an overhead hopper to manually pour the sand. This method worked relatively well, however it was reliant on the accuracy and patience of the user. To remove this human element, and hence to allow more uniform soil models to be prepared, an automatic sand pourer (shown in Figure 25) was developed which operates on similar principles to the overhead manual hopper. Different sized nozzles can be placed at the bottom of the hopper to control the flow rate and the drop height can be controlled through the program used to control the equipment. Calibration pours are conducted before pouring the model to determine the correct drop height and nozzle size in order to achieve the relative density desired. However, the eventual relative density achieved can be up to +/- 5% of the desired value but will be uniform throughout the model. Sand is poured in pairs of steps; each pass of the model along one axis is a single step. With up for 4mm/step being poured, often instrumentation cannot be located at precisely the desired depth. However, this is a small compromise compared to the benefits the automation process brings to model preparation. More details on the automatic sand pourer can be found in Madabhushi *et al*, 2006. This device was extensively calibrated for different relative density ranges as reported by Zhao et al, 2006 and Chian et al, 2010.

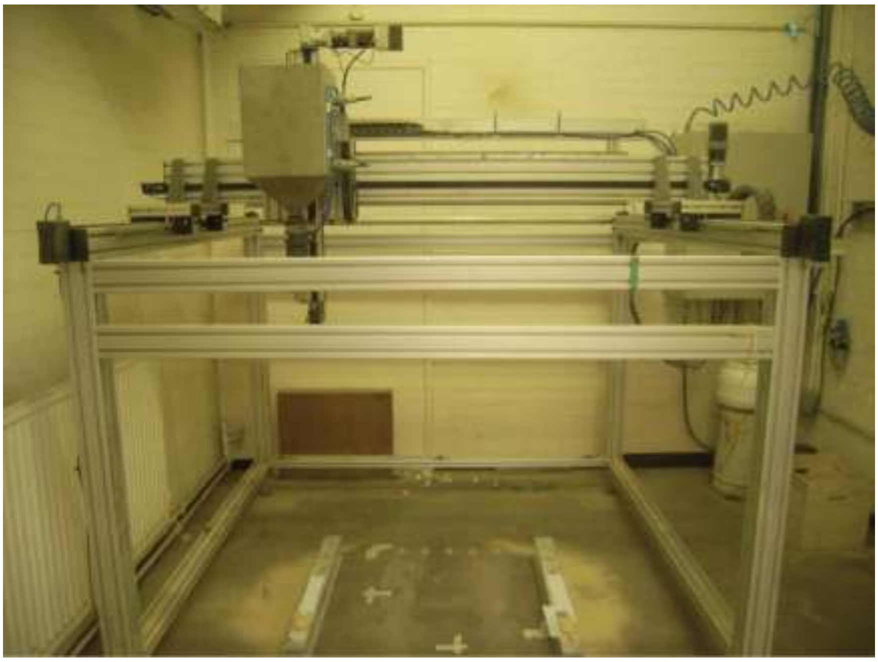

Figure 25: Automatic Sand Pourer

Testing Procedure

As discussed previously, the models are fully assembled prior to being loaded onto the centrifuge. The centrifuge at UCAM runs both dynamic and static tests however the SAM actuator does not remain on the centrifuge arm at all times, hence when it comes to dynamic tests the SAM actuator will be loaded prior to the model. Once the model is loaded the instrument connections are made to the data acquisition and any other air and water line connections are made. In addition, for the tests involving the high speed photography for PIV analysis, the camera needed to be focused prior to the tests.

Once all the connections were made between the model and the centrifuge and the camera focused, it was checked that all instruments were reading correctly and an image was taken at 1-g. As the centrifuge swung up it was normally held at a constant speed every 10g to check all the instruments were still reading correctly and to take a further image. These images are utilised to record how much the structure and soil move during swing-up.

When 50g was reached the swing-up data was uploaded and the SAM actuator and camera were prepared to fire the earthquake. For most tests the images were recorded at 1000 fps (frames per second) for about 1.5 seconds. The camera was triggered electronically at the same time as the data acquisition. Data was recorded at 4 kHz for 1.5 seconds during the normal sinusoidal earthquakes and for 3 seconds during the sine-sweep earthquakes. The data and images were uploaded immediately after each earthquake and both were checked to ensure they had recorded correctly.

Once all earthquakes were completed the centrifuge was stopped and one final image was taken to allow the motion of the soil and structure during swing-down to be determined.

PIV Analysis

PIV analysis was initially conceived for use in fluid mechanics to track the movement of fluid flows. The technique works on the principle of splitting an image into patches – each patch is then tracked from one image to the next.

As shown in Figure 26, the texture in each patch is compared to the texture within a set search zone in the secondary image. The location with the highest texture correlation is deemed to be the location of the patch in the secondary image, hence providing a displacement vector for that individual patch. The technique was initially adapted for use with geotechnical problems by White 2002 and was further advanced for use with dynamic geotechnical centrifuge testing by Cilingir and Madabhushi 2010.

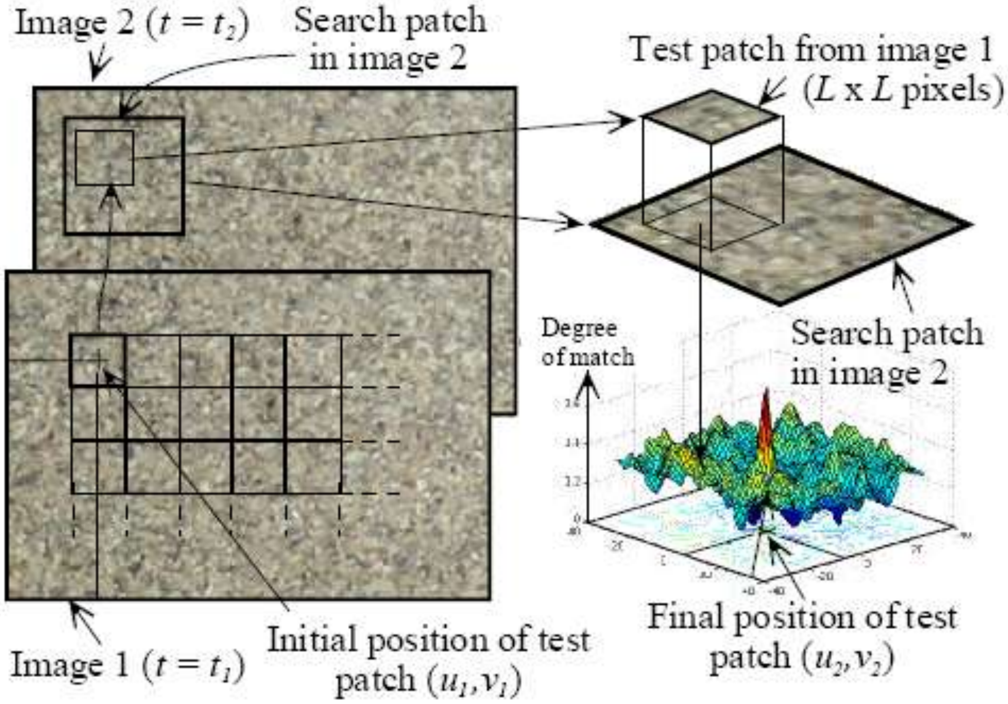

Figure 26: Principles of PIV Analysis (after White 2002)

Experimental Procedure-IFSTTAR

Model Preparation

Hostun Sand

The sand used by IFSTTAR is the same as that used by UCAM: Hostun sand type HN31. Its geotechnical characteristics are as follows:

Table 7 Geotechnical characteristics of Hostun HN31 sand

	Symbol	Value	Unit.
Maximum Void ratio	e_{max}	1,01	
Maximum Void ratio	e_{min}	0,636	
Maximum density	r_{dmax}	1620	kg/m^3
Minimum density	γ_{dmin}	1318	kg/m^3
Maximum specific weight	γ_{dmax}	15,89	kN/m^3
Minimum specific weight	γ_{dmin}	12,93	kN/m^3
Specific weight of grains	γ_S	26	kN/m^3
Grain density	γ_s	2650	kg/m^3

Automatic Sand Pourer

IFSTTAR pluviation device has been developed in 1987. It is a linear curtain hopper that moves automatically back and forth over the box. A slot at the bottom of the hopper forms the sand curtain. The tuning parameters for a given density are: the width of the slot, the height of falling (distance between the sand layer and the hopper slot) , the velocity of the displacement of the hopper, the number of journeys of the hopper over the box before changing its height.

For the SERIES JRA3 program the parameters of the pluviation where:

Table 8: Pluviation parameters at LCPC

	Slot	Falling Heigh	Horizontal velocity	Height tuning	I_D	γd
Low density	4 mm	57 cm	3.7 m/s	Every 2 journeys	51%	14.29 kN/m^3
High Density	4 mm	75 cm	10.8 m/s	Every 2 journeys	81%	15.23 kN/m^3

These pluviation parameters were controlled through a pluviation test at the beginning of the program using 2 density boxes placed at 5 cm from the container centre. The maximum absolute deviation of the density index between the two boxes was below 1% but placing the box at other locations showed the scatter of the density, especially nearer to the box end, was near 5%.

Figure 27: A View of the LCPC sand pluviation device

LCPC system generates a homogeneous layer in terms of thickness transversally as well as longitudinally. However:

- For convenience, the height of falling is not changed at each passage of the hopper; so that the density changes slightly because the height of falling is not absolutely constant (every one back and forth or every 2 back and forth),
- At the end of the box, the sand curtain traps a volume of air between the curtain and the box end. This generates turbulences that disturbs the sand curtains : while the hopper goes forth, the sand curtain is inclined to the back, increasing the quantity of sand deposited 20 cm from the container end and leaves a default in the sang layer near the container end wall. This is compensated manually by performing aborted pluviation path, closing the hopper slot after a 10 cm passage. This difficulty explains the 5% scatter of the density announced previously.

Testing procedure

Preparation of the sand container

The automatic sand pourer is used for the preparation of the sand container. The sand pouring is stopped when the request level for the positioning of an accelerometer is obtained. Placement of the accelerometer is made by hand and the location of the sensors is measured (X,Y,Z direction). After the test, during the dismantling, the final Z-position of each accelerometer is measured to evaluate the sensor settlement during the test. Once the final level is obtained the surface of the sand is levelled.

Preparation of the test in the centrifuge

Once the sand mass is obtained, the ESB box is put in place cautiously in the shaker that is in the basket of the centrifuge. The building is put in place with a mechanical system to optimised is positioning, once its position has been localised on the soil surface.

Frame equipped with laser sensors is put in place and all the connections of the sensors are made. Figure 28 illustrates the test at this stage.

Finally a miniature CPT device is put in place. The objective is to evaluate the homogeneity of the sand mass before and after the seismic events.

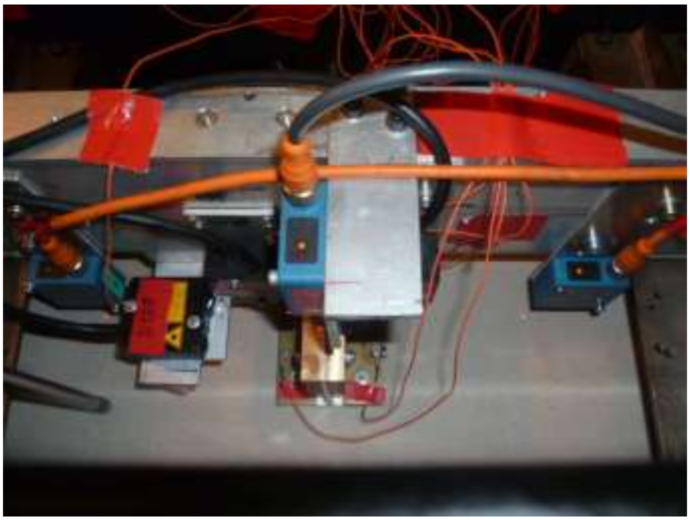

Figure 28: JRA3 test after the installation of the instrumentation

Consolidation cycle and CPT test

Before performing seismic tests, 3 cycles of consolidation at the request centrifuge acceleration are performed. Each consolidation cycle consisted in spin up the centrifuge up to the request centrifuge acceleration, maintain this acceleration during 5 minutes and spin down the centrifuge. Once the consolidation cycles are made a CPT test is performed at the request centrifuge acceleration. The centrifuge is then spin down and the CPT is dismantle before the centrifuge spin up and the seismic tests

Seismic tests

Once the request centrifuge acceleration is obtained the seismic tests are performed. Each test represent about 1s model and the time delay between two tests is about 1 minute. The acquisition of the data is made through the fast data acquisition system LMS for the accelerometer and the fast laser sensors, the low frequency acquisition system for the settlement measurement with low frequency laser sensor and the control system of the shaker for the table response in the 3 directions.

Once all the seismic test are finished the centrifuge is spin down and the CPT device is installed to measure, after the spin up of the centrifuge the resistance profile of the soil after the series of seismic event.

Test Details-UCAM

CH01

Date of Test: November 2009
Relative Density: 55%
Air hammer test in ESB box

Flight 1

Structure(s): No structure – free-field test
Earthquake 1: 50 Hz, 0.5 seconds, 2.00 V offset (07.7 g peak input acceleration)
Earthquake 2: 50 Hz, 0.5 seconds, 0.75 V offset (14.4 g peak input acceleration)
Earthquake 3: 60 Hz sine-sweep, 2.00 V offset (13.2 g peak input acceleration)

Flight 2

Structure(s): Type A1 (placed centrally on model)
Earthquake 1: 50 Hz, 0.5 seconds, 2.00 V offset (06.9 g peak input acceleration)
Earthquake 2: 50 Hz, 0.5 seconds, 0.75 V offset (13.9 g peak input acceleration)
Earthquake 3: 60 Hz sine-sweep, 2.00 V offset (13.5 g peak input acceleration)

Flight 3

Structure(s): Type A1 & Type A2 (placed as shown in Figure 29)
Earthquake 1: 50 Hz, 0.5 seconds, 2.00 V offset (06.5 g peak input acceleration)
Earthquake 2: 50 Hz, 0.5 seconds, 0.75 V offset (14.8 g peak input acceleration)
Earthquake 3: 60 Hz sine-sweep, 2.00 V offset (14.0 g peak input acceleration)

CH02

Date of Test: February 2010
Relative Density: 82%
Air hammer test in ESB box

Flight 1

Structure(s): No structure – free-field test
Earthquake 1: 50 Hz, 0.5 seconds, 2.00 V offset (07.5 g peak input acceleration)
Earthquake 2: 50 Hz, 0.5 seconds, 0.75 V offset (13.7 g peak input acceleration)
Earthquake 3: 60 Hz sine-sweep, 2.00 V offset (15.3 g peak input acceleration)

Flight 2

Structure(s): Type A1 (placed centrally on model)
Earthquake 1: 50 Hz, 0.5 seconds, 2.00 V offset (06.5 g peak input acceleration)
Earthquake 2: 50 Hz, 0.5 seconds, 0.75 V offset (14.7 g peak input acceleration)
Earthquake 3: 60 Hz sine-sweep, 2.00 V offset (15.4 g peak input acceleration)

Flight 3

Structure(s): Type A1 & Type A2 (placed as shown in Figure 29)
Earthquake 1: 50 Hz, 0.5 seconds, 2.00 V offset (06.7 g peak input acceleration)
Earthquake 2: 50 Hz, 0.5 seconds, 0.75 V offset (15.7 g peak input acceleration)
Earthquake 3: 60 Hz sine-sweep, 2.00 V offset (18.8 g peak input acceleration)

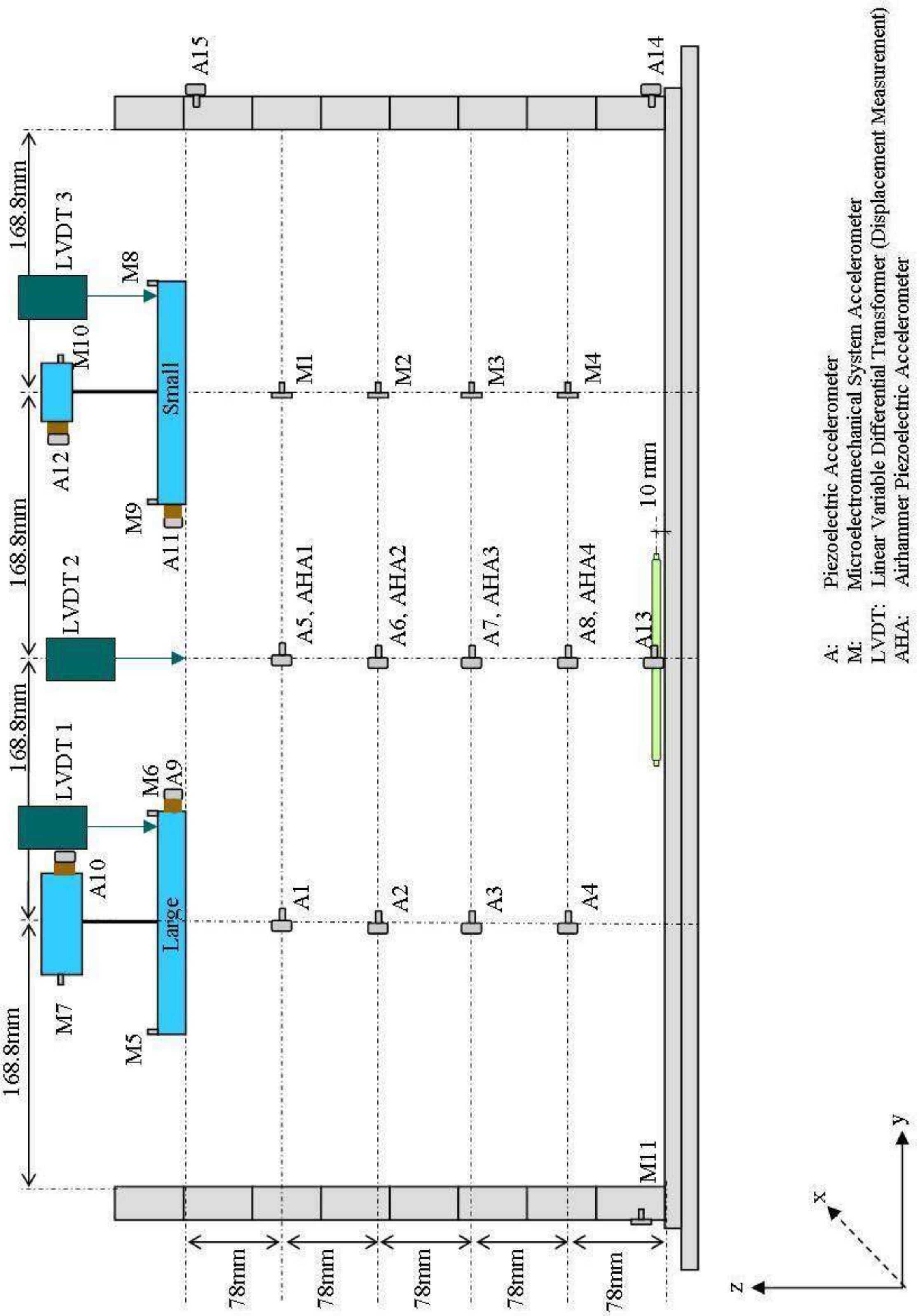

Figure 29: CH01 & CH02 Model Layout

CH03

Date of Test: March 2010
Relative Density: 50%
Air hammer test in ESB box

Flight 1

Structure(s): Type B1 & Type B2 (placed as shown in Figure 30)
Earthquake 1: 50 Hz, 0.5 seconds, 2.00 V offset (09.2 g peak input acceleration)
Earthquake 2: 50 Hz, 0.5 seconds, 0.75 V offset (16.6 g peak input acceleration)
Earthquake 3: 60 Hz sine-sweep, 2.00 V offset (17.2 g peak input acceleration)

CH04

Date of Test: August 2010
Relative Density: 74%
Air hammer test in ESB box
In this test the high speed camera was used to observe the movement of the large structure during the earthquake, hence no LVDT was placed onto the large structure as it would have obstructed the view of the camera.
Also, tekscan force sensors were attached to the base of the structures in an attempt to observe if lift-off was occurring. Due to the results from the force sensors not being adequate, the data is not discussed in this report.

Flight 1

Structure(s): Type B1 & Type B2 (placed as shown in Figure 31)
Earthquake 1: 50 Hz, 0.5 seconds, 2.00 V offset (10.0 g peak input acceleration)
Earthquake 2: 50 Hz, 0.5 seconds, 0.75 V offset (16.5 g peak input acceleration)
Earthquake 3: 60 Hz sine-sweep, 2.00 V offset (16.8 g peak input acceleration)
Earthquake 4: 40 Hz, 0.5 seconds, 0.75 V offset (10.6 g peak input acceleration)
Earthquake 5: 60 Hz sine-sweep, 1.00 V offset (24.1 g peak input acceleration)

CH05

CH05 was a test conducted during the commissioning of a new servo shaker at UCAM. The results from CH05 are not included within this report.

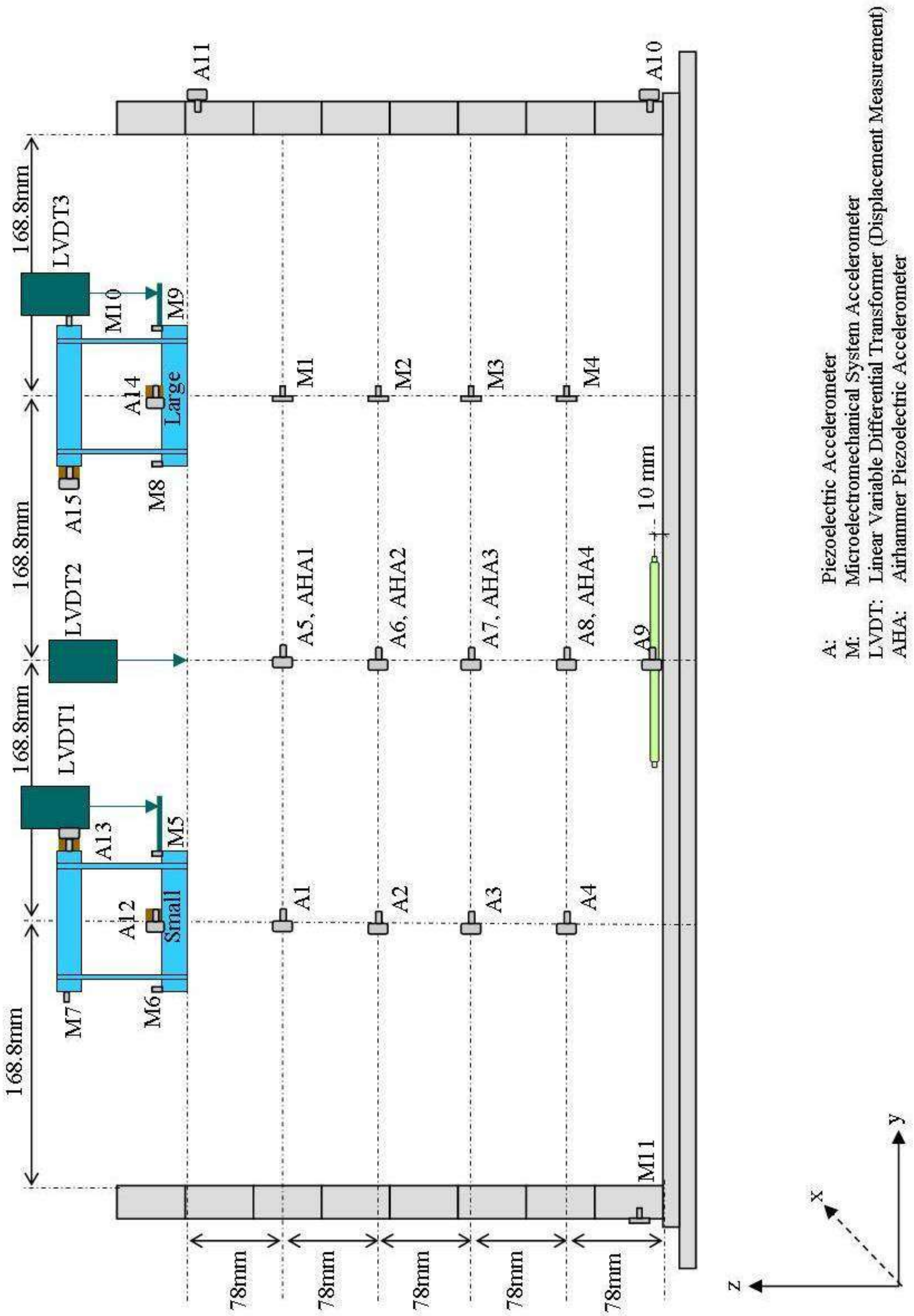

Figure 30: CH03 Model Layout

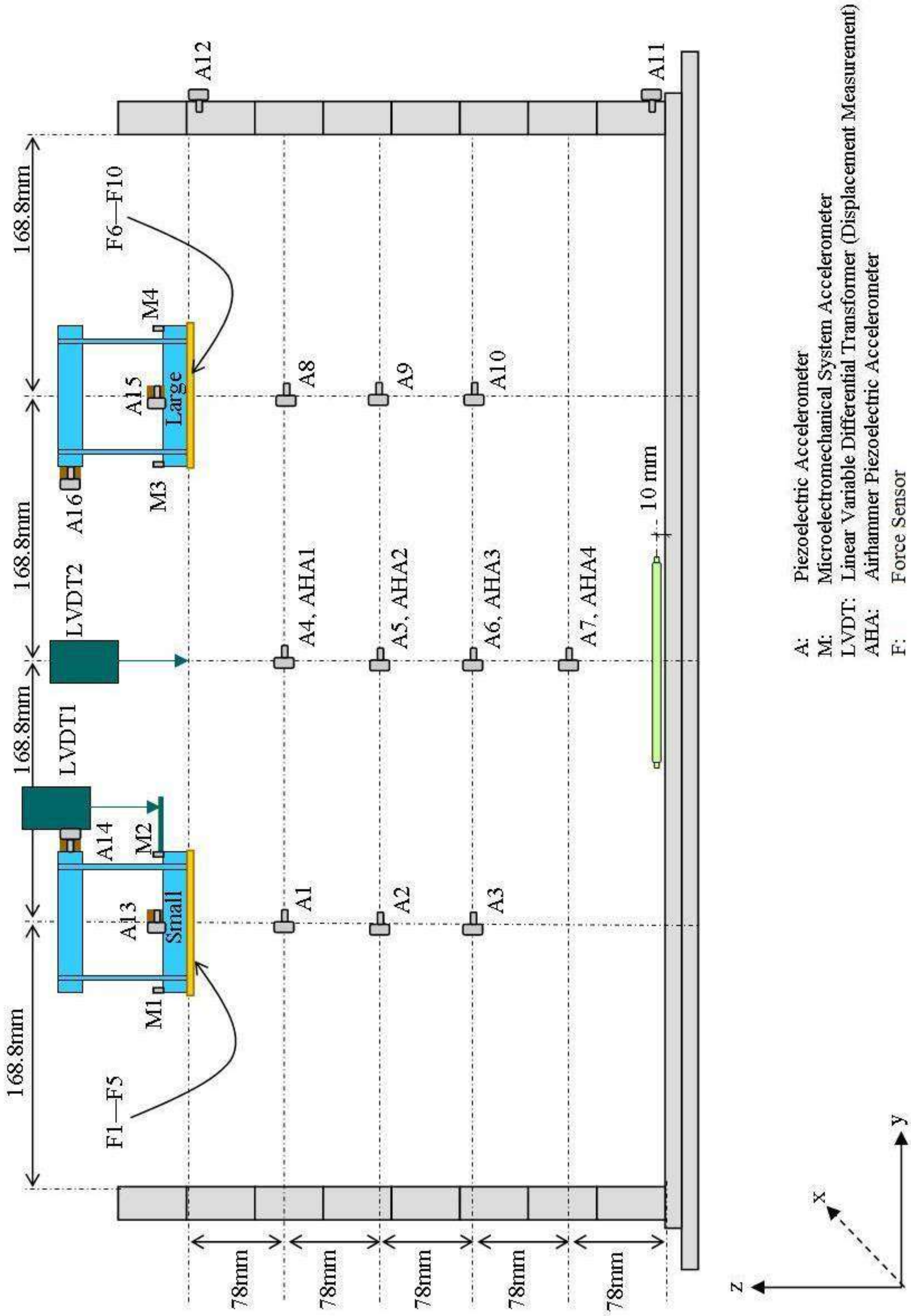

Figure 31: CH04 Model Layout

CH06

Date of Test: February 2011
Relative Density: 80%
PIV test in Window Box
Images captured at 500 fps

Flight 1

Structure(s): Type C1 (placed as shown in Figure 32)
Earthquake 1: 50 Hz, 0.5 seconds, 2.00 V offset (05.4 g peak input acceleration)
Earthquake 2: 50 Hz, 0.5 seconds, 0.75 V offset (12.9 g peak input acceleration)
Earthquake 3: 60 Hz sine-sweep, 2.00 V offset (09.6 g peak input acceleration)
Earthquake 4: 40 Hz, 0.5 seconds, 0.75 V offset (09.7 g peak input acceleration)
Earthquake 3: 60 Hz sine-sweep, 0.75 V offset (19.1 g peak input acceleration)

Flight 2

In this flight the soil was scraped to form ridges below the structure. This was done so that the structure would always have a static factor of safety of 1. The reason for this flight was to investigate how to maximise energy dissipation in the soil-structure interface.
Structure(s): Type C1 (placed as shown in Figure 32)
Earthquake 1: 50 Hz, 0.5 seconds, 2.00 V offset (06.0 g peak input acceleration)
Earthquake 2: 50 Hz, 0.5 seconds, 0.75 V offset (10.5 g peak input acceleration)
Earthquake 3: 60 Hz sine-sweep, 0.75 V offset (19.1 g peak input acceleration)

Flight 3

In this flight soil filled straws (representing pipes filled with an elastic material) were placed under the structure. The intention was similar to that for Flight 2 whereby the straws would squash as the structure rocked onto them and hence dissipate energy.
Structure(s): Type C1 (placed as shown in Figure 32)
Earthquake 1: 50 Hz, 0.5 seconds, 2.00 V offset (06.7 g peak input acceleration)
Earthquake 2: 50 Hz, 0.5 seconds, 0.75 V offset (12.0 g peak input acceleration)
Earthquake 3: 60 Hz sine-sweep, 0.75 V offset (20.8 g peak input acceleration)
Earthquake 4: 36 Hz, 0.5 seconds, 1.75 V offset (02.8 g peak input acceleration)
Earthquake 5: 36 Hz, 0.5 seconds, 0.75 V offset (05.4 g peak input acceleration)

CH07

Date of Test: May 2011
Relative Density: 50%
PIV test in Window Box
Images captured at 500 fps

Flight 1

Structure(s): Type C1 (placed as shown in Figure 32)
Earthquake 1: 50 Hz, 0.5 seconds, 2.00 V offset (05.1 g peak input acceleration)
Earthquake 2: 50 Hz, 0.5 seconds, 0.75 V offset (10.7 g peak input acceleration)
Earthquake 3: 60 Hz sine-sweep, 2.00 V offset (09.7 g peak input acceleration)
Earthquake 4: 41 Hz, 0.5 seconds, 0.25 V offset (11.0 g peak input acceleration)
Earthquake 5: 50 Hz sine-sweep, 0.75 V offset (12.3 g peak input acceleration)

Flight 2

In this flight soil filled straws (representing pipes filled with an elastic material) were placed under the structure. The reason for this flight was to investigate how to maximise energy dissipation in the soil-structure interface. The straws should squash as the structure rocked onto them and hence dissipate energy.
Structure(s): Type C1 (placed as shown in Figure 32)
Earthquake 1: 50 Hz, 0.5 seconds, 2.00 V offset (06.3 g peak input acceleration)
Earthquake 2: 50 Hz, 0.5 seconds, 0.75 V offset (12.9 g peak input acceleration)
Earthquake 3: 60 Hz sine-sweep, 2.00 V offset (09.5 g peak input acceleration)
Earthquake 4: 43 Hz, 0.5 seconds, 1.75 V offset (09.3 g peak input acceleration)
Earthquake 5: 50 Hz sine-sweep, 0.75 V offset (11.9 g peak input acceleration)

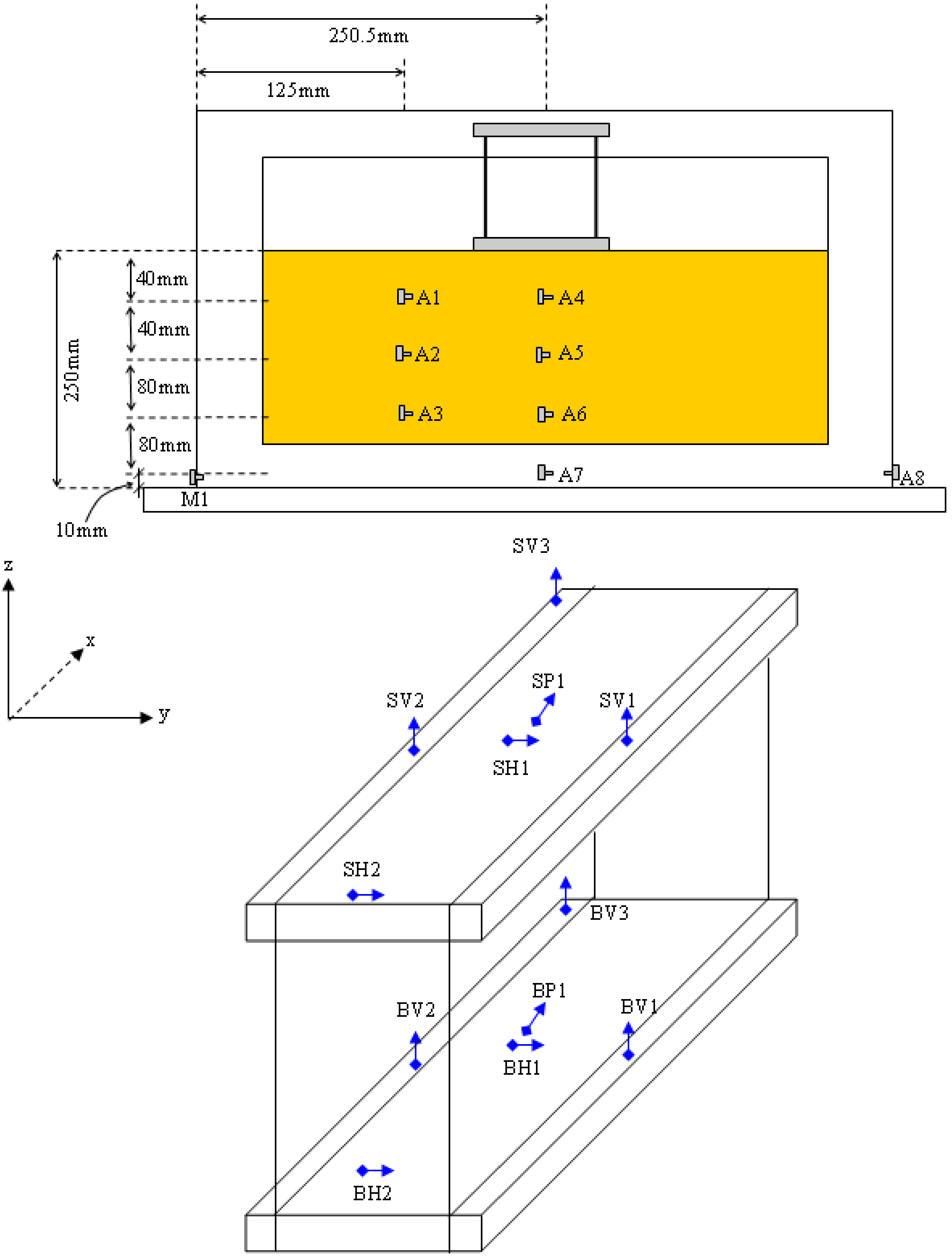

Figure 32: CH06 & CH07 Model Layout

CH08

Date of Test: July 2011
Relative Density: 50%
PIV test in Window Box
Images captured at 600 fps

Flight 1

Structure(s): Type C2 (placed as shown in Figure 33)
Earthquake 1: 50 Hz, 0.5 seconds, 2.00 V offset (05.0 g peak input acceleration)
Earthquake 2: 50 Hz, 0.5 seconds, 0.75 V offset (10.0 g peak input acceleration)
Earthquake 3: 60 Hz sine-sweep, 2.00 V offset (08.0 g peak input acceleration)
Earthquake 4: 60 Hz sine-sweep, 0.75 V offset (13.0 g peak input acceleration)
Earthquake 5: 60 Hz, 0.5 seconds, 1.00 V offset (15.0 g peak input acceleration)

Flight 2

In this flight soil filled straws (representing pipes filled with an elastic material) were placed under the structure. The reason for this flight was to investigate how to maximise energy dissipation in the soil-structure interface. The straws should squash as the structure rocked onto them and hence dissipate energy.

Structure(s): Type C2 (placed as shown in Figure 33)
Earthquake 1: 50 Hz, 0.5 seconds, 2.00 V offset (05.0 g peak input acceleration)
Earthquake 2: 50 Hz, 0.5 seconds, 0.75 V offset (10.0 g peak input acceleration)
Earthquake 3: 60 Hz sine-sweep, 2.00 V offset (08.0 g peak input acceleration)
Earthquake 4: 46 Hz, 0.5 seconds, 0.55 V offset (10.0 g peak input acceleration)
Earthquake 5: 54 Hz, 0.5 seconds, 0.55 V offset (14.0 g peak input acceleration)

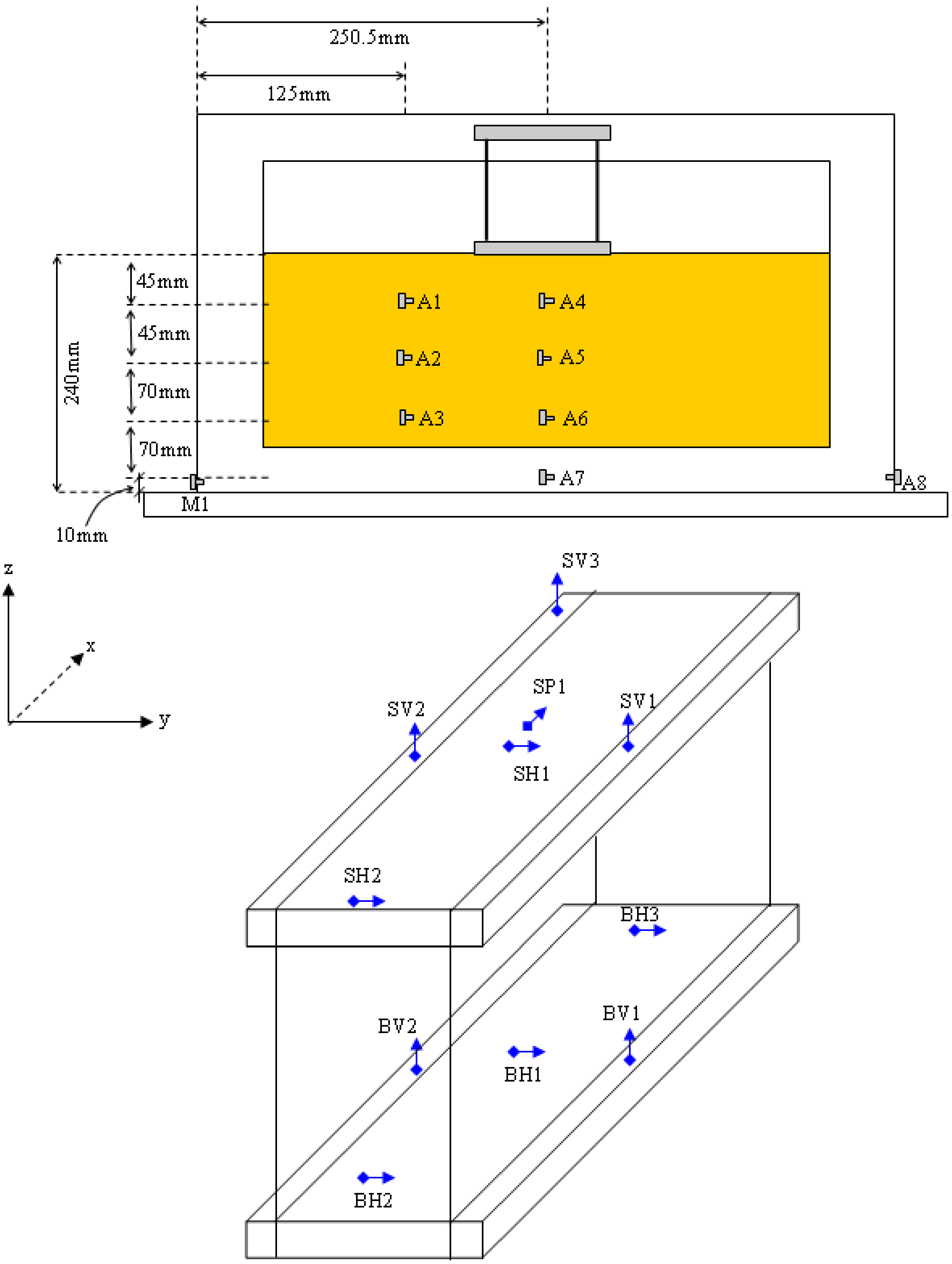

Figure 33: CH08 Model Layout

CH09

Date of Test: August/September 2011
Relative Density: 50%
PIV test in Window Box
Images captured at 1000 fps

Problems with the data acquisition system meant that two flights were conducted but the data failed to be collected on either flight.

Flight 3

Structure(s): Type C2 (placed as shown in Figure 34)
Earthquake 1: 50 Hz, 0.5 seconds, 2.00 V offset (06.0 g peak input acceleration)
Earthquake 2: 50 Hz, 0.5 seconds, 0.75 V offset (10.0 g peak input acceleration)
Earthquake 3: 50 Hz, 0.5 seconds, 0.75 V offset (11.0 g peak input acceleration)
Earthquake 4: 60 Hz sine-sweep, 0.75 V offset (16.0 g peak input acceleration)

Flight 4

Structure(s): Type D1b (placed as shown in Figure 34)
Earthquake 1: 50 Hz, 0.5 seconds, 2.00 V offset (data failed)
Earthquake 2: 50 Hz, 0.5 seconds, 0.50 V offset (12.0 g peak input acceleration)
Earthquake 3: 60 Hz sine-sweep, 0.50 V offset (17.0 g peak input acceleration)

Flight 5

Structure(s): Type D1a (placed as shown in Figure 34)
Earthquake 1: 50 Hz, 0.5 seconds, 2.00 V offset (06.0 g peak input acceleration)
Earthquake 2: 50 Hz, 0.5 seconds, 1.50 V offset (08.0 g peak input acceleration)
Earthquake 3: 50 Hz, 0.5 seconds, 1.00 V offset (10.0 g peak input acceleration)
Earthquake 4: 50 Hz, 0.5 seconds, 0.50 V offset (10.0 g peak input acceleration)
Earthquake 5: 60 Hz sine-sweep, 0.50 V offset (11.0 g peak input acceleration)

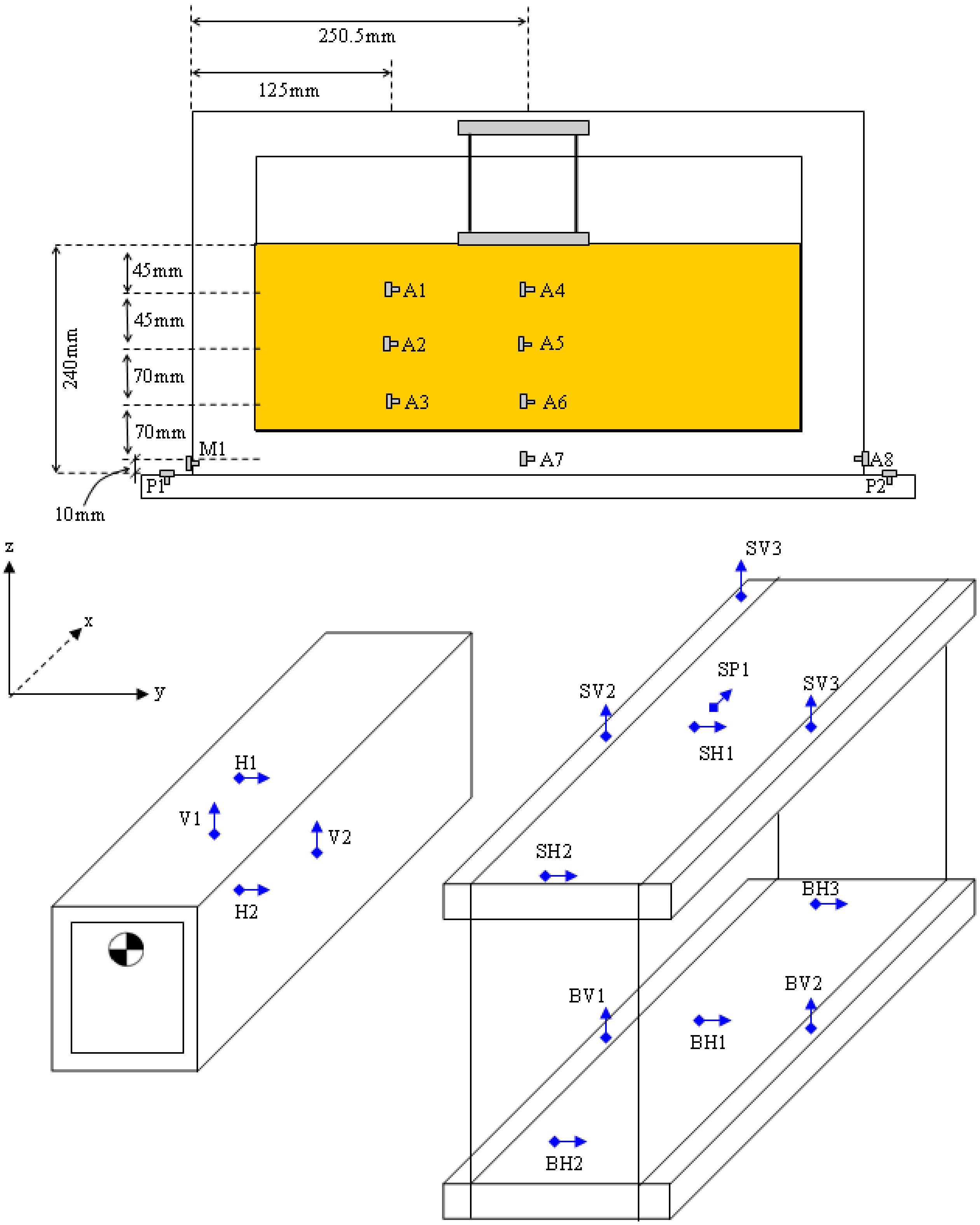

Figure 34: CH09 Model Layout

CH10

Date of Test: October 2011
Relative Density: 50%
PIV test in Window Box
Images captured at 1000fps

Flight 1

Structure(s): Type D2a (placed as shown in Figure 35)
Earthquake 1: 50 Hz, 0.5 seconds, 2.00 V offset (05.0 g peak input acceleration)
Earthquake 2: 50 Hz, 0.5 seconds, 0.75 V offset (10.0 g peak input acceleration)
Earthquake 3: 60 Hz sine-sweep, 2.00 V offset (09.0 g peak input acceleration)
Earthquake 4: 60 Hz sine-sweep, 0.75 V offset (14.0 g peak input acceleration)

Flight 2

The spring system used to hold the structure against the Perspex window was removed for this test to examine if it was impacting the free-response of the structure.
Structure(s): Type D2a (placed as shown in Figure 35)
Earthquake 1: 50 Hz, 0.5 seconds, 2.00 V offset (06.0 g peak input acceleration)
Earthquake 2: 50 Hz, 0.5 seconds, 0.75 V offset (11.0 g peak input acceleration)
Earthquake 3: 50 Hz, 0.5 seconds, 1.40 V offset (08.0 g peak input acceleration)
Earthquake 4: 50 Hz, 0.5 seconds, 1.70 V offset (07.0 g peak input acceleration)
Earthquake 5: 50 Hz, 0.5 seconds, 1.55 V offset (08.0 g peak input acceleration)
Earthquake 6: 50 Hz, 0.5 seconds, 1.85 V offset (06.0 g peak input acceleration)
Earthquake 7: 40 Hz, 0.5 seconds, 1.68 V offset (04.0 g peak input acceleration)
Earthquake 8: 40 Hz, 0.5 seconds, 1.41 V offset (04.0 g peak input acceleration)

Flight 3

Structure(s): Type E (placed as shown in Figure 35)
Earthquake 1: 50 Hz, 0.5 seconds, 2.00 V offset (06.0 g peak input acceleration)
Earthquake 2: 50 Hz, 0.5 seconds, 0.75 V offset (12.0 g peak input acceleration)
Earthquake 3: 50 Hz, 0.5 seconds, 1.40 V offset (08.0 g peak input acceleration)
Earthquake 4: 50 Hz, 0.5 seconds, 1.70 V offset (07.0 g peak input acceleration)
Earthquake 5: 40 Hz, 0.5 seconds, 1.00 V offset (05.0 g peak input acceleration)
Earthquake 6: 50 Hz, 0.5 seconds, 0.20 V offset (14.0 g peak input acceleration)

CH11

Date of Test: November 2011
Relative Density: 80%
PIV test in Window Box
Images captured at 1000fps

Flight 1

Structure(s): No structure – free-field test
Earthquake 1: 50 Hz, 0.5 seconds, 2.00 V offset (05.0 g peak input acceleration)
Earthquake 2: 50 Hz, 0.5 seconds, 2.00 V offset (05.0 g peak input acceleration)
Earthquake 3: 50 Hz, 0.5 seconds, 0.75 V offset (10.0 g peak input acceleration)
Earthquake 4: 60 Hz sine-sweep, 0.75 V offset (15.0 g peak input acceleration)

Flight 2

Structure(s): Type E (placed as shown in Figure 35)
Earthquake 1: 50 Hz, 0.5 seconds, 2.00 V offset (05.0 g peak input acceleration)
Earthquake 2: 50 Hz, 0.5 seconds, 0.75 V offset (10.0 g peak input acceleration)
Earthquake 3: 60 Hz sine-sweep, 0.75 V offset (16.0 g peak input acceleration)
Earthquake 4: 50 Hz, 0.5 seconds, 0.20 V offset (12.0 g peak input acceleration)

Flight 3

The spring system used to hold the structure against the Perspex window was removed for this test to examine if it was impacting the free-response of the structure.
Structure(s): Type D2a (placed as shown in Figure 35)
Earthquake 1: 50 Hz, 0.5 seconds, 2.00 V offset (05.0 g peak input acceleration)
Earthquake 2: 50 Hz, 0.5 seconds, 0.75 V offset (10.0 g peak input acceleration)
Earthquake 3: 50 Hz, 0.5 seconds, 1.40 V offset (07.0 g peak input acceleration)
Earthquake 4: 50 Hz, 0.5 seconds, 1.70 V offset (06.0 g peak input acceleration)
Earthquake 5: 50 Hz, 0.5 seconds, 1.85 V offset (06.0 g peak input acceleration)
Earthquake 6: 50 Hz, 0.5 seconds, 0.95 V offset (05.0 g peak input acceleration)
Earthquake 7: 50 Hz, 0.5 seconds, 2.00 V offset (05.0 g peak input acceleration)
Earthquake 8: 40 Hz, 0.5 seconds, 1.35 V offset (05.0 g peak input acceleration)
Earthquake 9: 40 Hz, 0.5 seconds, 1.00 V offset (05.0 g peak input acceleration)
Earthquake 10: 60 Hz sine-sweep, 0.75 V offset (16.0 g peak input acceleration)

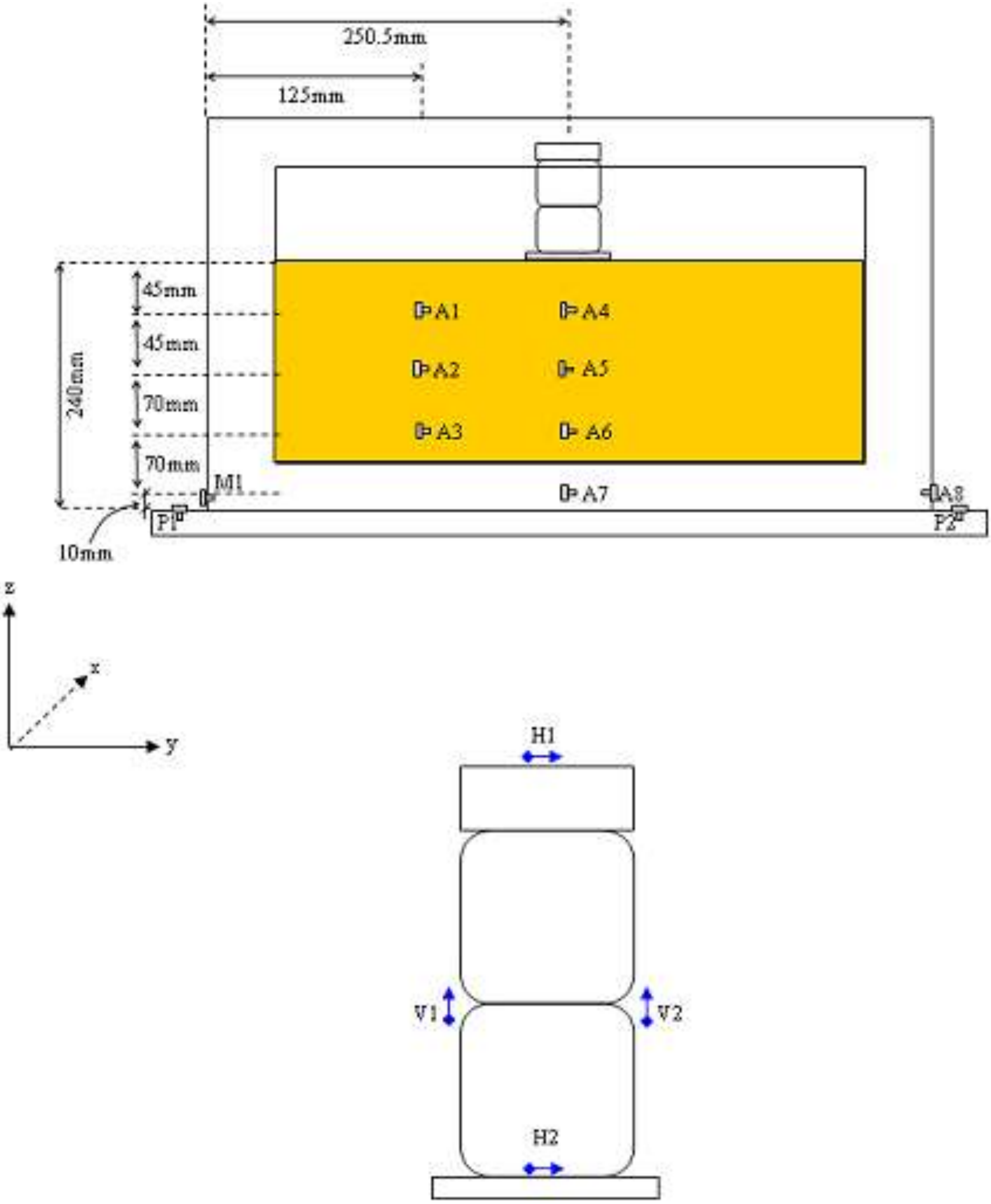

Figure 35: CH10 & CH11 Model Layout

Test Details-IFSTTAR

Inputs selected

Two series of test have been performed. The first series of tests has been based on the seismic inputs given by UCAM. The two first input named T1F1E1 and T1F1E2 have been given by UCAM. These signals contain energy around 50 and 150 Hz at the model scale (1 and 3Hz at the prototype scale). A third input has been selected by IFSTTAR: an 50Hz sine with an Arias intensity around that of the T1F1E2 signal in the 20-60Hz frequency range. The objective is to highlight an effect of the 150Hz component. Table 9 gives some characteristics of these inputs.

Table 9: Characteristics of the input

Input	T1F1E1	T1F1E2
Cambridge Arias Intensity	**1.087**	**5.088**
Corresponding Arias Intensity of a pure sine 50 Hz	**0.996** [40 cycles 2,75g +11HCR]	**4.743** [40 cycles + 6 g +11HCR]
Arias Intensity of UCAM input filtered 20-60Hz		**2.743**
Corresponding Arias Intensity of a pure sine 50 Hz		**2.52** [20 cycles + 6 g +11HCR)]

HCR : number of half cycles of ramps at the beginning and end of the signal, shared in two parts

The reference signal in the case of the T1F1E1 and T1F1E2, that take into account the capacities of the shaker are presented in the figures 36 and 37.

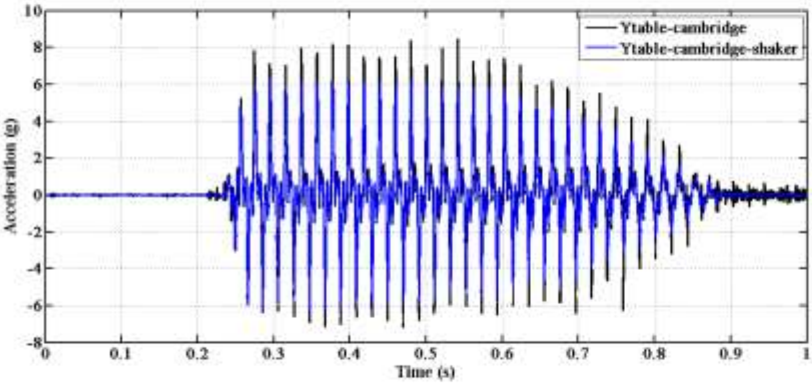

(a)

Figure 36a T1F1E1 – signal given by UCAM (black) and the reference signal for the IFSTTAR test (in blue) (a) time

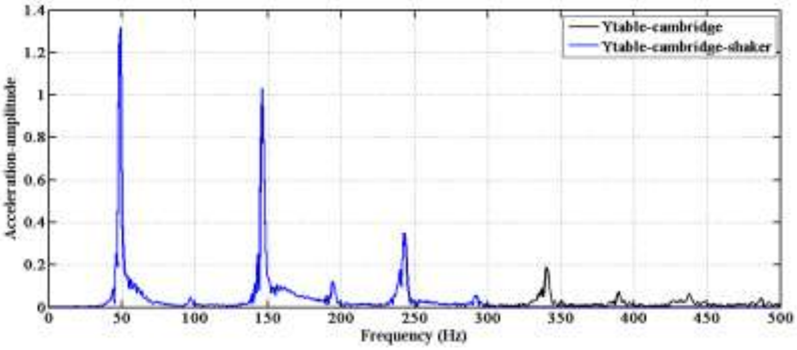

(b)

Figure 36b T1F1E1 – signal given by UCAM (black) and the reference signal for the IFSTTAR test (in blue) (b) frequency representations.

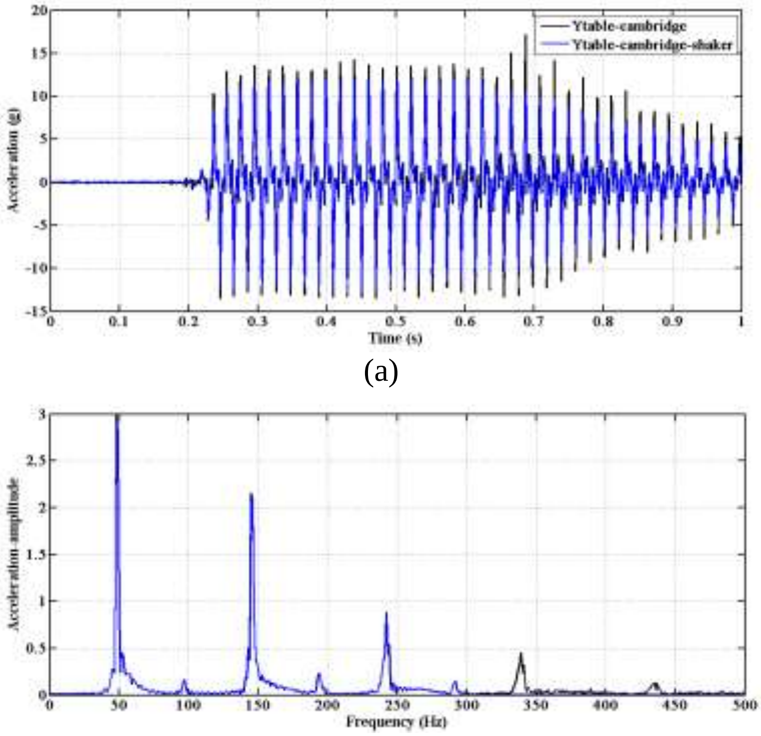

(a)

(b)

Figure 37 T1F1E2 – signal given by UCAM (black) and the reference signal for the IFSTTAR test (in blue) (a) time and (b) frequency representations.

After this first series of tests a second series of tests has been performed with large frequency band earthquakes: Landers earthquake and Northridge earthquake. One of the objectives was the determination of the response frequencies of the soil column and the building versus the input.

Table 10 summarized the tests that have been performed. It is followed by some examples of the test definition files for:

-free filed test (same configuration for the tests JRA3_1_1, JRA3_1_2, JRA3_2_1 and JRA3_2_2)

-test with a building and a uniform soil layer (without vertical fast laser sensor and accelerometer at 20mm depth in the soil– same configuration for the tests JRA3_5_1, JRA3_5_2, JRA3_5_3, JRA3_6_1; JRA3_8_2)

-test with a building and a uniform soil layer (without vertical fact laser sensor– same configuration for the tests JRA3_7_2, JRA3_7_3, JRA3_8_1)

-test with two layers (JRA3_10_1 and JRA3_11_1)

Note that some slight differences exist between each test concerning the acquisition channel, the position of the sensor on the building, in the soil (measured value) etc. However each test has its own description file

Table 10: JRA3 tests performed by IFSTTAR centre

Test	D_r [%]	γ_d [kN.m^3]	Vertical static stress (kPa)	event
JRA3_1_1	57%	14.47	Free filed	T1F1E1-2dB/ T1F1E1-2dB/ T1F1E2/ Sin50Hz6gh
JRA3_1_2	57%	14.47	Free filed	T1F1E1/ T1F1E1/ T1F1E2/ Sin50Hz6gh
JRA3_2_1	80,1	15.2	Free filed	T1F1E1-2dB/ T1F1E1-2dB/ T1F1E2/ Sin50Hz6gh
JRA3_2_2	80,1	15.2	Free filed	T1F1E1/ T1F1E1/ T1F1E2/ Sin50Hz6gh
JRA3_3	57%	14.47		Static bearing capacity measurement
JRA3_4	80,1	15.2		Static bearing capacity measurement
JRA3_5_1	57	14.47	100	T1F1E1/ T1F1E1/ T1F1E2/ Sin50Hz6gh
JRA3_5_2	57	14.47	100	T1F1E1/ T1F1E1/ T1F1E2/ Sin50Hz6gh
JRA3_6_1	80,1	15.2	100	T1F1E1/ T1F1E1/ T1F1E2/ Sin50Hz6gh
JRA3_6_2	80,1	15.2	100	T1F1E1/ T1F1E1/ T1F1E2/ Sin50Hz6gh
JRA3_7_1	57	14.47	300	T1F1E1/ T1F1E1/ T1F1E2/ Sin50Hz6gh
JRA3_7_2	57	14.47	300	T1F1E1/ T1F1E1/T1F1E1/ T1F1E2/ Sin50Hz6gh
JRA3_7_3	57	14.47	300	T1F1E1/ T1F1E1/T1F1E1/ T1F1E2/ Sin50Hz6gh
JRA3_8_1	80.1	15.2	300	T1F1E1/ T1F1E1/ T1F1E2/ Sin50Hz6gh
JRA3_8_2	80.1	15.2	300	T1F1E1/ T1F1E1/ T1F1E2/ Sin50Hz6gh
JRA3_9_1	57	14.47	100 & 300	T1F1E1/ T1F1E1/ T1F1E2/ Sin50Hz6gh
JRA3_10_1	57/80.1	14.47/15.85	300	Landers -10dB/ Landers -0.5dB/ Landers 0dB/ Northridge/ Sinus 50Hz
JRA3_11_1	57/80.1	14.47/15.85	100	Landers -10dB/ Landers -0.5dB/ Landers 0dB/ Northridge/ Sinus 50Hz
JRA3_12_1	57	14.47	100	Landers -10dB/ Landers -0.5dB/ Landers 0dB/ Northridge/ Sinus 50Hz
JRA3_13_1	80.1	15.2	100	Landers -10dB/ Landers -0.5dB/ Landers 0dB/ Northridge/ Sinus 50Hz
JRA3_14_1	80.1	15.2	300	Landers -10dB/ Landers -0.5dB/ Landers 0dB/ Northridge/ Sinus 50Hz

Project	**Model**	**Experimentation**	**Page 1/3**
SERIES JRA3	Free Field – Low density – box 1	seriesjra3_1_1	

Soil Bed Characteristics

Pluviation parameters	**Fente**	**Height**	**Horiz. Freq.**	**Height tuning**		
	4 mm	57 cm	6,7 Hz	Each B-F		
Soil	**emin**	**emax**	**gammadmin**	**gammadmax**	**Id**	**gammad**
Hostun sand HN31	0.64	1.01	12.93 N/m^3	15.89 kN/m^3	51.00 %	14.29 kN/m^3

- conteneur : ESB inside dimensions 0,80 (L)x0,35 (w) x 0,41 (h) m
- Reduction factor : 1/50th – centrifuge gravity : 50 g

Sensor table

Acquisition Chanel	Sensor	Theoretical Position	Positive Direct.	Real coordinates at set-up			Real Position after shocks
				X cm	Y cm	Z cm	Z cm
1	B&K81	Y table	+pivot				
2- OUT	B&K70	table center					
3	B&K68	Lateral- 78 mm /bottom	+pivot	17	62,5	33,4	33,7
4	B&K69	Central- 78 mm / bottom	+pivot	17,5	40	33,3	33,8
5	B&K73	Central- 156 mm/ bottom	+pivot	17,5	38,5	26,2	26,6
6	B&K72	Lateral - 156 mm / bottom	+pivot	17,7	63,5	26,7	26,9
7	B&K75	Central - 234 mm/ bottom	+pivot	17,5	40	17,8	18,3
8	B&K74	Lateral - 234 mm / bottom	+pivot	17,3	63	18,2	18,9
9 - OUT	B&K78	Central- 312 mm/ bottom	+pivot	16,5	40,5	10,8	11,8
10	B&K76	Lateral - 312 mm / bottom	+pivot	17,2	63	11,2	11,8
11	B&K82	Box - 78 mm /bottom	+door				
12	B&K83	Box - 156 mm /bottom	+door				
13	B&K84	Box - 234 mm /bottom	+door				
14	B&K85	Box - 312 mm /bottom	+door				
15 - OUT	B&K86	Box - 410 mm /bottom	+door				

Settlement and penetrometer records

Settlement record file	Penetrometer record files
Before shaking	
seriesJRA3_1_1_settl_rel.xls	seriesjra3_1_1_V1.xls seriesjra3_1_1_V2.xls seriesjra3_1_1_V3.xls
During and after shaking	
seriesJRA3_1_1_settl_rel.xls	seriesjra3_1_1_P1.xls seriesjra3_1_1_P2.xls seriesjra3_1_1_P3.xls

Project	**Model**	**Experimentation**	**Page 2/3**
SERIES JRA3	Free Field – Low density – box 1	seriesjra3_1_1_1 à seriesjra3_1_1_4	

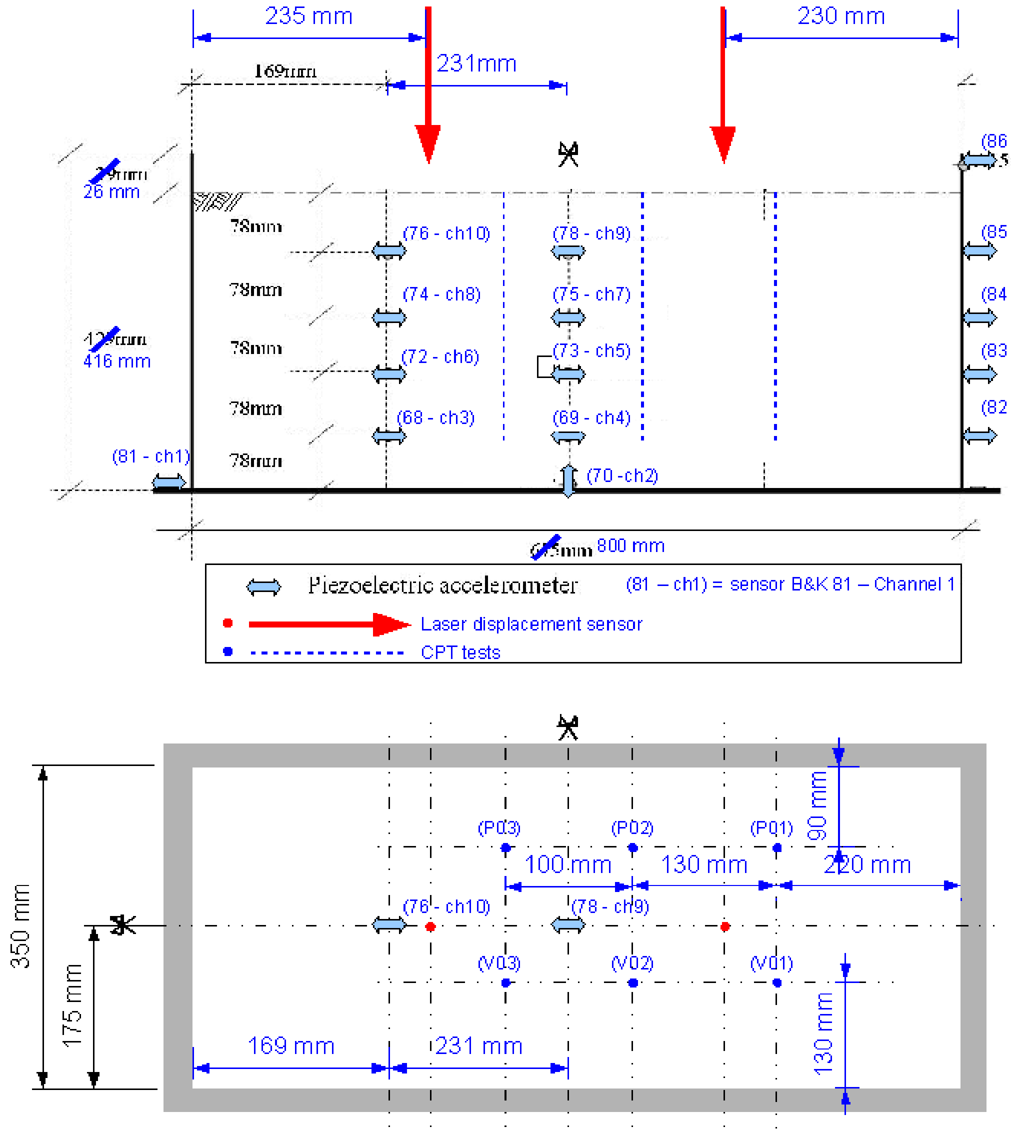

Sensor theoretical positions (see table above for real position measured during setup)

Earthquake sequences and file numbers

Date : 2009, Decembre 16trh

File Name	Input sismique
Seriesjra3_1_1_1	T1F1E1 – 2 dB
Seriesjra3_1_1_2	T1F1E1 – 2 dB
Seriesjra3_1_1_3	T1F1E2
Seriesjra3_1_1_4	Sine 50gc 50hz 6g

Project	Model	Experimentation	Page 1/2
SERIES JRA3	Building 100 kPa – Low density – box 2	**seriesjra3_5_2**	

Soil Bed Charactéristics an model

Pluviation parameters	**Fente**	**Height**	**Horiz. Freq.**	**Height tuning**		
	4 mm	57 cm	6,7 Hz	Each B-F		
Soil	**emin**	**emax**	**gammadmin**	**gammadmax**	**Id**	**gammad**
Hostun sand HN31	0.64	1.01	12.93 kN/m^3	15.89 kN/m^3	51,00%	14,45 kN/m^3

- Conteneur : ESB inside dimensions 0,80 (L)x0,35 (w) x 0,41 (h) m
- Reduction factor : 1/50th – **centrifuge gravity : 50 g**
- Buidling model : contact stress 100 kPa (see drawings file) -
- Mass of the model (verified March 26th,2010) = 1344,3 g – Stress at soil level at 50 g : 103,02 kPa

Sensor table

(Z is measured from the top ring of the box – The soil surface is initialy is 26 mm below)

Acquisition Chanel	Sensor	Theoretical Position	Positive Direct.	Real coordinates at set-up			Real Position after shocks
				X cm	Y cm	Z* cm	Z * cm
1	B&K81	Y table	+pivot				
2	B&K70	Ytable center	+pivot				
3	B&K68	Lateral - 78 mm /bottom	+pivot	18	62.7	32.5	32,7
4	B&K69	Central - 78 mm / bottom	+pivot	17,5	40	32,4	32,6
5	B&K73	Central- 156 mm/ bottom	+pivot	17,7	40	25	25,6
6	B&K72	Lateral - 156 mm / bottom	+pivot	18	62,7	25,1	25,5
7	B&K75	Central- 234 mm/ bottom	+pivot	17,1	39,8	16,5	17,3
8	B&K74	Lateral- 234 mm / bottom	+pivot	17,5	63	17	17,5
9	B&K79	Central- 312 mm/ bottom	+pivot	17,3	40	8,2	9,5
10	B&K76	Lateral- 312 mm / bottom	+pivot	17,3	63,1	9	9,7
11	B&K82	Box - 78 mm /bottom	+door				
12	B&K83	Box - 156 mm /bottom	+door				
13	B&K84	Box - 234 mm /bottom	+door				
14	B&K85	Box - 312 mm /bottom	+door				
15	B&K86	Box - 410 mm /bottom	+door				
16	B&K95	Central - just above B1K70	+pivot	17,5	40	39,7	39,8
17	B&K87	Building – Bottom Vertical (pivot)	+up				
18	B&K88	Building – Bottom Vertical (door)	+up				
19	B&K89	Building – Bottom Horizontal (door)	+pivot				
20	B&K90	Building – Top Horizontal (pivot)	+pivot				
25	με displ. sensor	Building – Top Horizontal					
21	B&K91	On the displacement sensor	+door				

CPT Test	Settlement
seriesjra3_5_2_V1.xls before shaking seriesjra3_5_2_P1.xls after shaking	seriesjra3_5_2_settl.xls

Project	Model	Experimentation	Page 2/2
SERIES JRA3	Building 100 kPa – Low density – box 2	seriesjra3_5_2	

Sensor theoretical positions (see table above for real positions measured during setup)

Sensor positions on building model

Earthquake sequences and file numbers - Date : March 23h, 2010

File name	Input
rseriesjra3_5_2_1.mat	shake T1F1E1
rseriesjra3_5_2_2.mat	shake T1F1E1 – 9 dB
rseriesjra3_5_2_3.mat	shake T1F1E1
rseriesjra3_5_2_4.mat	shake T1F1E1 – 9 dB
rseriesjra3_5_2_5.mat	shake T1F1E1
rseriesjra3_5_2_6.mat	shake T1F1E2
rseriesjra3_5_2_7.mat	shake sin50gc50Hz

Project	**Model**	**Experimentation**	**Page 1/2**
SERIES JRA3	Building 300 kPa – High Density – box 1	**seriesjra3_8_1**	

Soil Bed Charactéristics an model

Pluviation parameters	**Fente**	**Height**	**Horiz. Freq.**	**Height tuning**		
	4 mm	75 cm	22 Hz	Every 2 Back &Forth		
Soil	**emin**	**emax**	**gammadmin**	**gammadmax**	**Id**	**gammad**
Hostun sand HN31	0.64	1.01	12.93 kN/m^3	15.85 kN/m^3	80.10%	15.2 kN/m^3

- Conteneur : ESB inside dimensions 0,80 (L)x0,35 (w) x 0,41 (h) m
- Reduction factor : 1/50th – centrifuge gravity : 50 g
- Buidling model : contact stress 100 kPa (see drawings file) -

Sensor table

Acquisition Chanel	Sensor	Theoretical Position	Positive Direct.	Real coordinates at set-up			Real Position after shocks
				X cm	Y cm	Z cm	Z cm
1	B&K81	Y table	+pivot				
2	B&K70	Ytable center	+pivot				
3	B&K68	Central- 78 mm /bottom	+pivot	17,5	62,3	33,5	33,7**
4	B&K69	Lateral - 78 mm / bottom	+pivot	17,3	39,8	32,5	32,8**
5	B&K73	Central- 156 mm/ bottom	+pivot	17,5	40,1	25,7	25,9**
6	B&K72	Lateral - 156 mm / bottom	+pivot	18	63	25,1	25,3**
7	B&K75	Central- 234 mm/ bottom	+pivot	17,5	4à	17,6	17,7**
8	B&K74	Lateral- 234 mm / bottom	+pivot	18	63	17,2	17,1**
9	B&K79	Central- 312 mm/ bottom	+pivot	17,2	40,2	10,4	10,6**
10	B&K76	Lateral- 312 mm / bottom	+pivot	17	60,2	9,6	9,6**
11	B&K82	Box - 78 mm /bottom	+door				
12	B&K83	Box - 156 mm /bottom	+door				
13	B&K84	Box - 234 mm /bottom	+door				
14	B&K85	Box - 312 mm /bottom	+door				
15	B&K86	Box - 410 mm /bottom	+door				
16	B&K95	Central - just above B1K70	+pivot	17	39,4	40,4	40,4
17	B&K96	Building Door side – Bottom Vertical	+up				
18	B&K97	Building pivot side – Bottom Vertical	+up				
19	B&K99	Building – Bottom Horizontal pivot	+pivot				
20	B&K90	Building – Top Horizontal pivot	+pivot				
25	$\mu\varepsilon$ displ. sensor	Building – Top Horizontal	+pivot				
21	B&K91	On the displacement sensor	+door				
22	B&K92	Lateral 20mm below the fondation	+pivot	17,2	63	3,5	3,6**
23	B&K93	Central 20mm below the fondation	+door	18	40,5	4,6	5**

- Care ; Z is measured from the top of the box but the top of the sand is 26 mm below the top ring (see drawing)
- ** 2 mm have been added for difference in operator procedure

Settlement and penetrometer records

CPT Test .xls files and associated txt files	Settlement
seriesjra3_8_1_V1 – before shaking seriesjra3_8_1_P1 – after shaking	seriesjra3_8_1_settl

Project	**Model**	**Experimentation**	**Page 2/2**
SERIES JRA3	Building 300 kPa – High Density – box 1	seriesjra3_8_1	

Sensor theoretical positions (see table above for real positions measured during setup)

Sensor positions on building model

Earthquake sequences and file numbers - Date : April 30th, 2010

File Name	Input sismique
rseriesjra3_8_1_1	T1F1E1 shot 1
rseriesjra3_8_1_2	T1F1E1 shot 2
rseriesjra3_8_1_3	T1F1E2 shot 1
rseriesjra3_8_1_4	Sine 50 gc 50 Hz 6 gh

Project	**Model**	**Experimentation**	**Page 1/2**
SERIES JRA3	Structure 300 kPa Low Density on top - thikness B/2- High density below	**seriesjra3_10_1**	

Soil Bed Charactéristics an model

Pluviation parameters	**Slot**	**Height**	**Horiz. Freq.**	**Height tuning**		
	4 mm	57 cm	6,4 Hz	Each B-F	ep = 4 last cm	
	4 mm	75 cm	22 Hz	Every 2 B-F	ep = 37 cm	
Soil	**emin**	**emax**	**gammadmin**	**gammadmax**	**Id**	**gammad**
Hostun sand HN31	0.64	1.01	12.93 kN/m^3	15.85 kN/m^3	57.%	14.45 kN/m^3
Hostun sand HN31	0.64	1.01	12.93 kN/m^3	15.85 kN/m^3	81.%	15.23 kN/m^3

- Conteneur : ESB inside dimensions 0,80 (L)x0,35 (w) x 0,41 (h) m
- Reduction factor : 1/50th – centrifuge gravity : 50 g
- Buidling model : contact stress 300 kPa - Frequency on rigid base 50 Hz

Sensor table

DAS Chanel	Sensor B&K	Theoretical Position	Theori.Depth/ cm		Positive Direct.	Real coordinates at set-up			Real Position after shocks
			/top box	/sand surface		X cm	Y cm	Z cm	Z cm
1	101	Y table - Trigger			+pivot				
2	70	Ytable center of the box	-41,6	-39	+pivot	17,5	39,3	40,2	NR
3	91	Central - just above B1K70	-40,6	-38	+ pivot	17,5	19,3	33,5	33,5
4	68	Central - 78 mm /bottom	-33,8	-31,2	+pivot	17,6	15,2	32,8	NR
5	69	Lateral door- 78 mm / bottom	-33,8	-31,2	+pivot	17,5	39	26,5	26,6
6	74	Central- 156 mm/ bottom	-26	-23,4	+pivot	17,5	16,5	25,6	25,65
7	75	Lateral door - 156 mm / bottom	-26	-23,4	+pivot	17,5	39,7	18,6	18,8
8	80	Central - 234 mm/ bottom	-18,2	-15,6	+pivot	17,3	17,5	17,7	17,75
9	82	Lateral door - 234 mm / bottom	-18,2	-15,6	+pivot	21	39,7	9,3	9,3
10	88	Central - 312 mm/ bottom	-10,4	-7,8	+pivot	17,5	16,5	10,9	11,2
11	89	Lateral door - 312 mm / bottom	-10,4	-7,8	+pivot	17	39,5	4,1	4,8
12	92	Beneath foundation door -10 mm/surface	-3,6	-1	+ pivot	17,5	16,7	4	4
13	93	Lateral pivot -10 mm/surface	-3,6	-1	+ pivot	NR	NR	NR	NR
14	84	Box - 78 mm /bottom			+door				
15	85	Box - 156 mm /bottom			+door				
16	86	Box - 234 mm /bottom			+door				
17	87	Box - 312 mm /bottom			+door				
18	94	Box - 410 mm /bottom			+door				
19	102	Structure 300 kPa - Bottom Vertical			+up				
20	103	Structure 300 kPa - Bottom Vertical			+up				
21	104	Structure 300 kPa - Bottom Horizontal			+pivot				
22	107	Structure 300 kPa - top c-o-m Horizontal			+door				

Settlement and penetrometer records

CPT Test .xls files and associated txt files	Settlement
seriesjra3_10_1_data/ seriesjra3_10_1_sensors / seriesjra3_10_1_comments	seriesjra3_10_1_data_sttl/ seriesjra3_10_1_sensors_sttl / seriesjra3_10_1_comments_sttl

Project	**Model**	**Experimentation**	**Page 2/2**
SERIES JRA3	Structure 300 kPa	**seriesjra3_10_1**	

	Low Density on top - thikness B/2- High density below		

Sensor theoretical positions (see table above for real positions measured during setup)

Sensor positions on building model

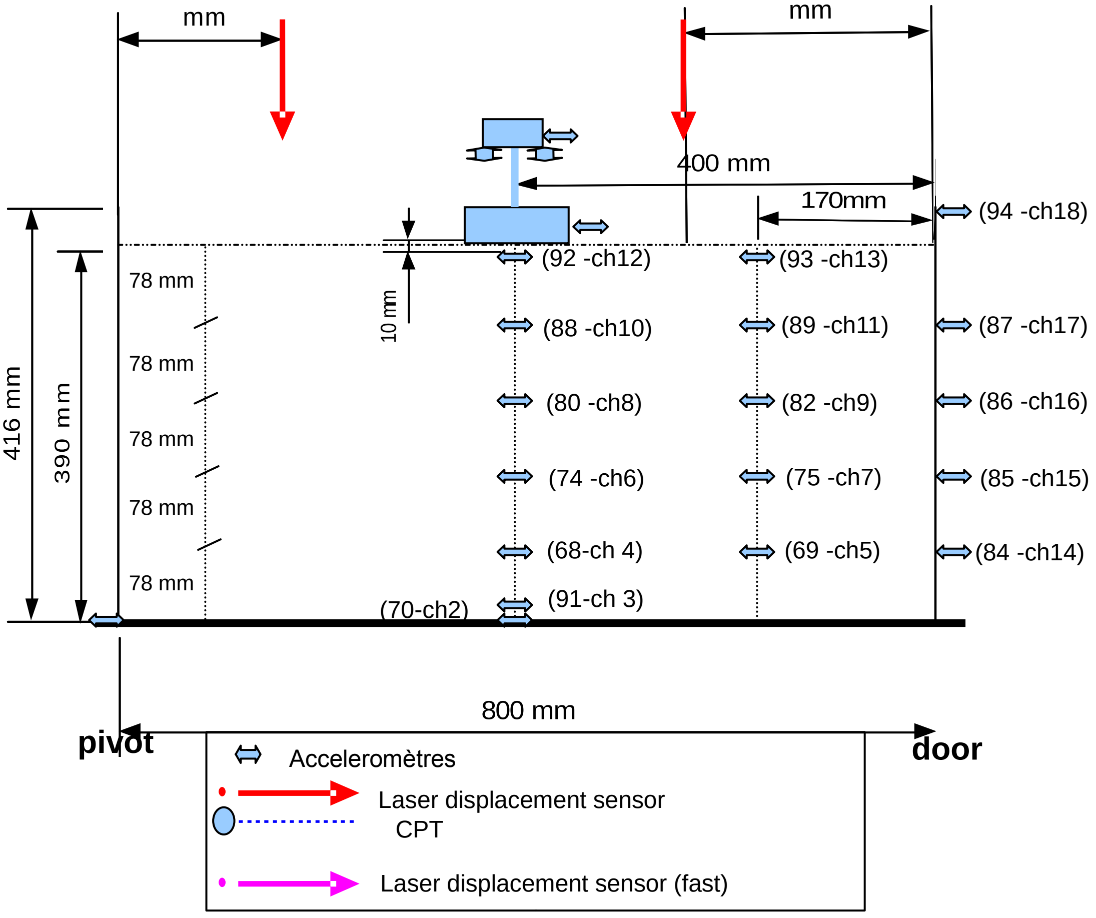

Structure

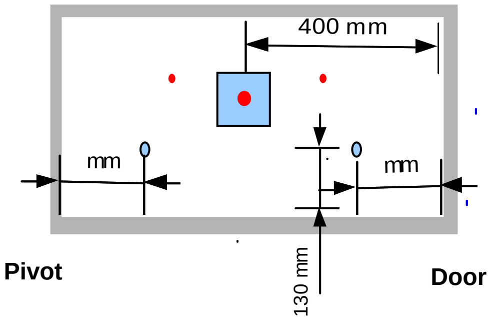

Structure 300

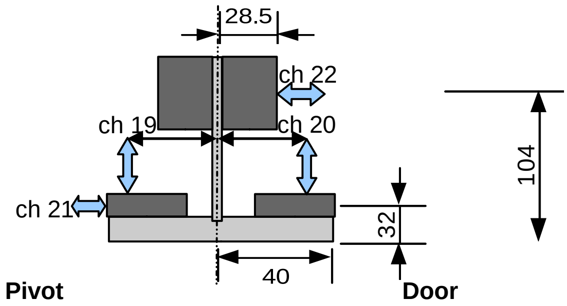

Earthquake sequences and file numbers - Date : June 14th, 2011

File Name	Input sismique
Jra3_10_1_2	Landers -10 db
Jra3_10_1_3 NR	Landers -0,5 db
Jra3_10_1_4	Landers -0,5 db
Jra3_10_1_5	Landers -0db
Jra3_10_1_6	Northridge
Jra3_10_1_7	Sinus 50Hz

Results

The results from the PIV tests are still under analysis and hence the majority of the following discussion will be based on results from the Phase I tests conducted in he ESB box and using type A & B structures.

Soil Density

Settlements-UCAM

The most apparent impact of varying relative density is the changes in settlement of the structures. Naturally, the looser sand will allow more settlement than the denser sand as shown in Figure 38. The small structure on the loose sand settled excessively, by nearly 180mm (prototype scale). Even in the dense sand, the structure settled by approximately 50mm. It should be noted that the structural settlements plotted in Figure 38 were measured using an LVDT located on the edge of the structure. Due to the poor performance of LVDTs at high frequency only the final settlement can be accurately determined from the data. Also, due to the LVDT being located on the outer edge of the foundation, the settlement value recorded will be the maximum final settlement over the base of the foundation.

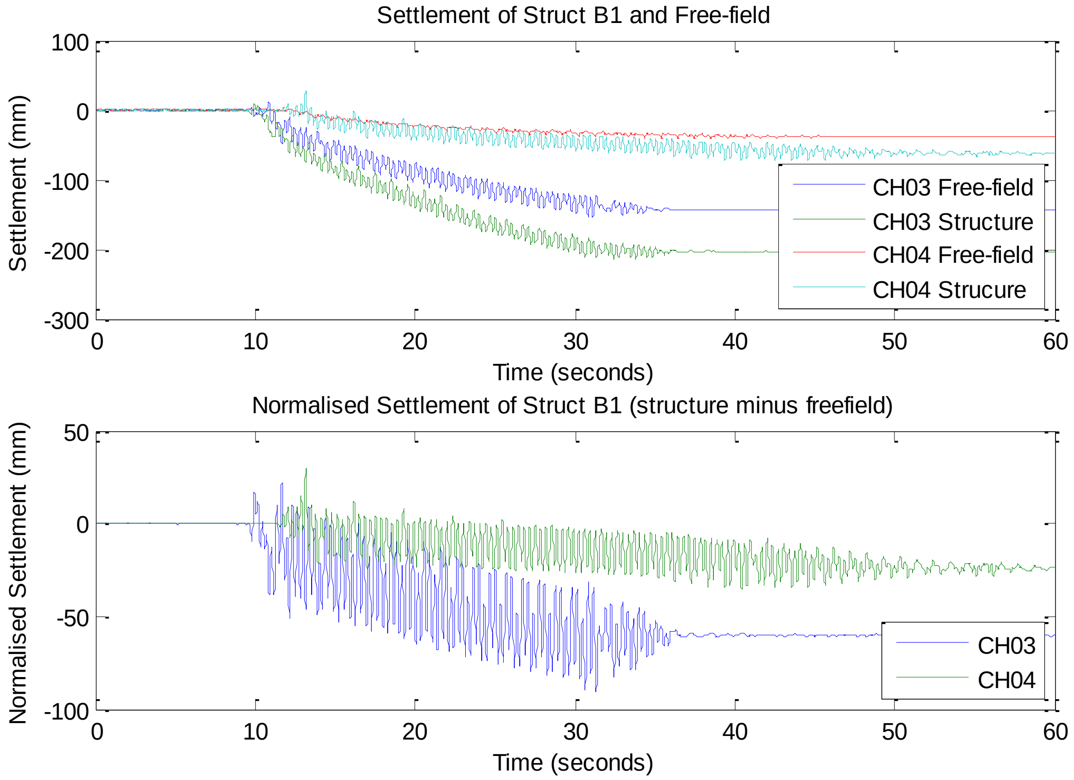

Figure 38: Relative Density Effects on Settlement (CH03 & CH04 EQ2 Struct B1. Prototype Scale

Assuming uniform settlement occurs across an entire foundation, the most serious impact of large settlements of foundations during earthquakes is damage caused to services (water, waste, electricity etc) that run into the building. Therefore, what is perhaps more relevant than total settlement is the amount of settlement relative to the free field, as shown in the bottom plot of Figure 38. Naturally the structure sited on the loose sand will still settle more relative to the free field; however the differential settlement is 54mm. This value is still relatively large, although it is not so excessive that services etc. could not be designed to cope with such a differential settlement. The structure located on the dense sand experiences a differential settlement of only 22mm. Total settlement of the structure on the loose sand was four times that for the dense sand, however, the differential settlement was only twice as much. This initial analysis implies that allowing the footings to rock and consequently settle more does not result in differential settlements between the structure and the free field, which could not be catered for during design. However, the problem arises when the ground varies below the footing itself and differential settlements occur beneath the foundation. Potentially, ground improvement work would be required prior to construction to ensure the ground being built on is uniform enough to prevent undesirable levels of differential settlement.

The movement at the edges of the structure during the earthquake will, at times, exceed the final settlement, as observed in Figure 38, due to the rocking of the foundation. However, the maximum movement can not be determined from this figure due to the LVDTs poor dynamic response (the true value will be larger than that recorded). As the foundation rotates down on one side and uplifts on the other, it will load the soil beneath the edge of the foundation more heavily than at the centre. This will result in more deformation at the edge of the footing compared to at the centre. This is why the final settlement profile under a rocking foundation can appear humped - although such observations were not possible in these tests. The maximum foundation movement, as opposed to the final settlement value, will be the critical value when designing shallow foundations for seismically active zones.

If ground improvement works were to be carried out, it would be important to know to what depth the works would be required to go to. Once the analysis of the PIV images is completed, information on the depth of the zone of influence of a rocking structure should be obtainable.

Settlements-IFSTTAR

The settlements of the soil and the structures have been measured by low frequency laser sensors. In the case of the soil it is based on the average settlement measuring by 2 laser sensors. For the measurement of the building settlement, it is located at the top of the building and corresponds approximately to the centre of the foundation. The low frequency laser sensors only enable the recording the settlement induces by an event. The tables below gives the results obtained for the soil and the relative settlement between the soil in free filed condition and the building.

In the case of the soil settlement the medium dense sand settles more than the dense sand and that for all the successive events. The settlement of the soil column in its virgin state is only represented by the settlement recorded during the first event T1F1E1. Considering the medium value, the medium dense sand settles almost 3 times more than the dense sand. The following identical event T1F1E1, in both cases induces lower settlement indicating none negligible effect of the first event. In the case of the event T1F1E2, which arias intensity is more than 4.5 times higher than that of the T1F1E1 input, the settlement is non negligible compare the previous induced by the T1F1E1 events. It can be noticed that the sine does not implies large settlement. This remark is consistent with the energy and frequency content of this signal (its frequency is smaller than the frequency response of the soil column that can be estimated around 2.75 Hz from seismic tests – these results are not presented in this report)

Such as for the first series of test the settlement recorded during the second series of test (seismic tests) are larger for the medium dense sand.

Table 11: Settlement of the soil column during successive events (prototype scale)

ID	Concerned boxes	Events	Average settlement (mm)	Standard deviation (mm)	Min/max (mm)
57%	JRA3_1_1	T1F1E1-n°1	41	± 7	32/52
	JRA3_1_2	T1F1E1-n°2	11	± 3	6/15
	JRA3_5_2	T1F1E1-n°3*	8.5	± 0.5	8/9
	JRA3_7_3	T1F1E2-n°1	63	± 3	60/69
		Sine	5		3/10
	JRA3_12_1	Landers -10dB**	10	-	-
		Landers -5dB**	18	-	-
		Landers 0dB**	37	-	-
		Northridge -10dB**	45	-	-
		Sine**	5	-	-
80%	JRA3_2_1	T1F1E1-n°1	15	± 2	14/19
	JRA3_2_2	T1F1E1-n°2	7	± 3	4/10
	JRA3_6_1	T1F1E1-n°3***	3		
	JRA3_6_1	T1F1E2-n°1	25	± 3	21/28
	JRA3_6_2	Sine	0	± 0	0/1
	JRA3_13_1	Landers -10dB	4.5	±0.5	4/5
	JRA3_14_1	Landers -5dB	7	±0	7
		Landers 0dB	15	±0	14/15
		Northridge -10dB	18	±1	17/19
		Sine	0	±0	0

*It concerns only the tests JRA_5_2 and JRA3_7_3, this additional event do not has a relevant effect on the following events.

** It concerns only one test so only one value.

*** *It concerns only the tests JRA_2_1, this additional event do not has a relevant effect on the following events.

As previously mentioned by UCAM one interesting point is the relative settlement between the soil in the free field and the building. Table 12 illustrates this point. In this case average value are not given because of the reduce number of data. Instead of that all the data are given. From these results it can be noticed that the discrepancy of the data in the case of the first series of test performed on the lighter building (100 kPa building) do not enable to conclude on the effect of the density on the relative settlement in the case of this building. However in the case of the heavier building (300kPa) the relative settlement is slightly higher for the medium dense sand. Nevertheless the most significant effect on the relative settlement comes from the building weight. If the initial state is considered (first T1F1E1 event) the relative settlement in the medium dense sand is from 3.5 to 2.5 higher for the 300 kPa building. In the case of the dense it is 2.8 to 3.9 higher for the 300 kPa building.

In addition an interesting point is that contrary to the soil settlement that is negligible during the sine event performed in the first series of test, the relative settlement is not negligible. This remark is in accordance with the frequency content of the input and the response frequency of the building. In the case of the soil the frequency of the sine input is far away from the soil response frequency inducing a small effect in terms of settlement. At the contrary the response frequency of the soil-building system and the sine are closed together inducing larger interaction that seems to induce larger settlement of the building and thus larger relative settlement.

In the case of the seismic events the effect of the density and the building weight are comparable. It indicates that the input frequency has a major effect on the relative settlement. Considering the energy content of the input the results are consistent with the fact that a input with non negligible energy around the frequency response of the soil-building system will induce larger settlement.

Table 12: Differential settlement between the structure and the free filed settlement during successive events (prototype scale)

Building		100 kPa			300 kPa	
Soil		57%	80%	57%/80%	57%	80%
Concerned tests		JRA3_5_1 JRA3_5_2	JRA3_6_1 JRA3_6_2		JRA3_7_31	JRA3_8_1 JRA3_8_2
Successive inputs	T1F1E1-n°1	29/41	22/31		102	85/87
	T1F1E1-n°2	11/19	8/15		46	28/29
	T1F1E1-n°3*	8/			32	
	T1F1E2-n°1	36/69	34/38		110	99/100
	Sine	9/18	7/8		37	22/27
Concerned tests		JRA3_12_1	JRA3_13_1	JRA3_11_1		JRA3_14_1
Successive inputs	Landers -10dB	8	5		13	8
	Landers -5dB	17	9		26	13
	Landers 0dB	28	18		55	22
	Northridge -10dB	18	14		20	14
	Sine	25	0		0	22

*It concerns only the tests JRA_5_2

Effect of density on the Moment-Rotation Loops - UCAM

One method that can be used to examine soil structure interaction is the moment-rotation plot which links the moment applied by the foundation to the soil with the foundation rotation. It is possible to determine an approximation of the moment that is applied to the sand by the foundation by summing two contributory factors. Firstly and most significantly, the moment applied by the d'Alembert force experienced by the superstructure and secondly, the moment applied by the rotational mass moment of inertia of the foundation and superstructure. The latter of these however does not add significantly to the moment. The rotation of the footing is determined from the double integral of the acceleration traces provided by the vertical MEMS accelerometers located on either side of the base of the structure. Due to problems (acceleration drift) in performing the double integral of acceleration traces to get displacement information, a large amount of filtering is required, and this has the potential to reduce the peak amplitude of the displacement. This simply means that the moment-rotation loops produced should be stretched horizontally by an unknown factor. However, if the same filtering methods are applied every time a moment-rotation loop is produced, then comparisons can still be made between them. In future work the image analysis of the PIV tests will allow the rotations to be calculated more accurately.

It is interesting to examine the changes in the moment-rotation loops when different relative densities of sand are tested. The moment rotation loops for the Type B2 structure during Tests CH03 (50%) & CH04 (80%) are shown in Figure 39.

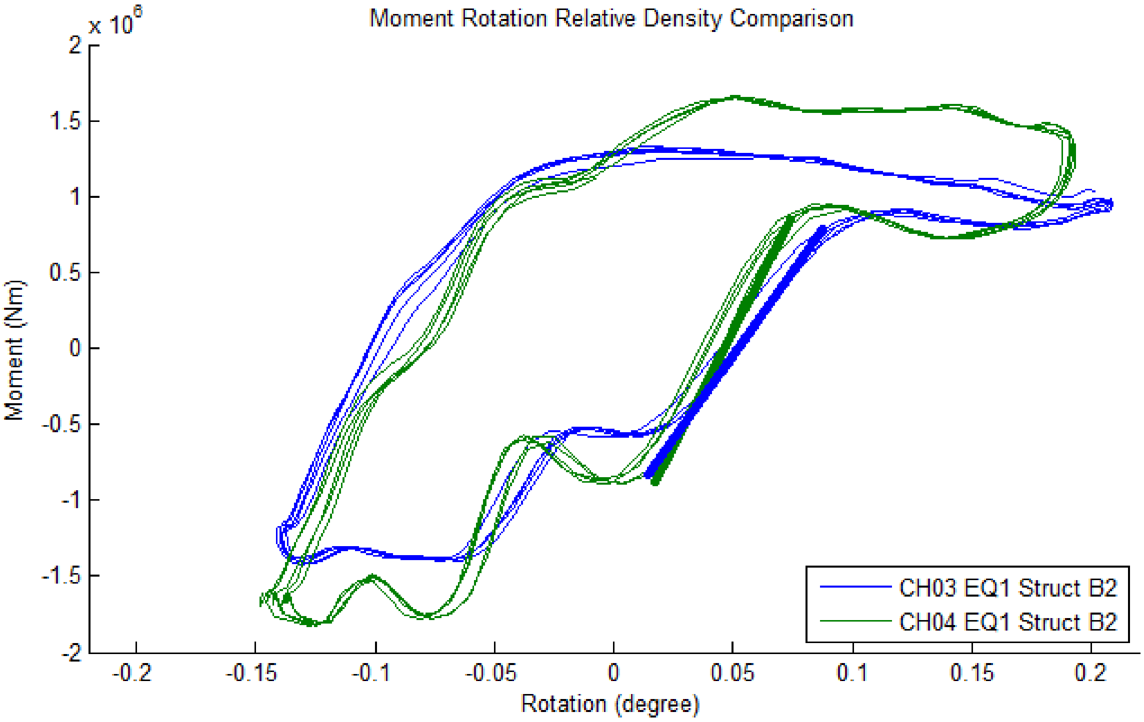

Figure 39: Relative Density Effects on Moment Rotation (CH03 & CH04 EQ1 Struct B2)

From Figure 39, it can be observed that at low moments and low rotations (when strains are small), the response of the footing on the denser sand is stiffer (steeper) than that on the looser sand. However, as rotations increase and hence shear strains increase, the stiffness decreases to a similar level irrespective of initial relative density. In the denser sand, a larger moment is required to cause the levelling out of the moment-rotation loop. The levelling off of the moment-rotation loops would imply that the foundations are lifting off at one side and experiencing increased rotation with constant moment being applied. In future analysis of the PIV data it will be possible to examine further the lift off of the structure during earthquake loading. Once the centre of rotation is known, the restoring moment from the self-righting characteristic of the structure can be added to the moment-rotation loops, which could potentially remove the ‘noise’ that is superimposed on top of the current loops. The area within the moment-rotation loops provides an indication of the energy being dissipated in the rocking of the structure. Figure 39 would imply that more energy is being dissipated under the footing on the denser sand. This could be due to the structure located on the looser sand settling (densifying the sand) as well as rocking, whereas the structure on the denser sand will dissipate energy primarily through rocking.

Effect of density on the Moment-Rotation Loops - IFSTTAR

The effect of the soil density on the moment rotation loops can be illustrated by the moment rotation loops obtained during the seismic event T1F1E1, T1F1E2, and sinus. For respectively the 100 kPa and the 300 kPa building, the density effect is illustrated on Figures 40 to 41.

It can be noticed that a double integration process has been used to obtained the moment-rotation loops from the acceleration measurement on the building. However this procedure has been verified based on the comparison of the horizontal displacement of the top mass of the building by an fast laser sensor and the double integration of two accelerometer (one glued on the top mass and one glued on the laser sensor). The difference was lower than 8% between the two methods (when the residual displacement measured by the laser sensor is removed).

In the case of the lighter building the effect of the soil density on the moment-rotation loop is not clearly highlighted. Especially for the input with the lower level, T1F1E1, the moment rotation loops are more or less superposed. In the case of the T1F1E1 and sine inputs, the soil-structure interaction seems less dissipative with the denser sand especially for the sine input. However concerning the stiffness of the soil-building system the discrepancy are in the order of the discrepancy obtained from reproducibility tests that are not presented in this report.

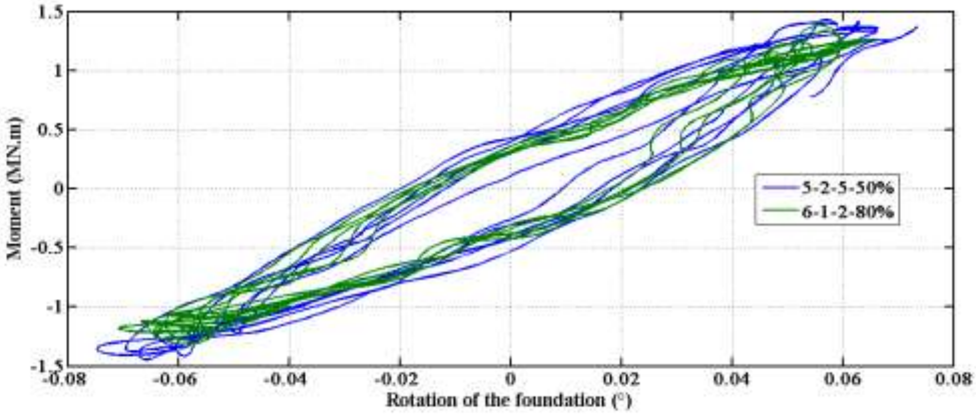

(a)

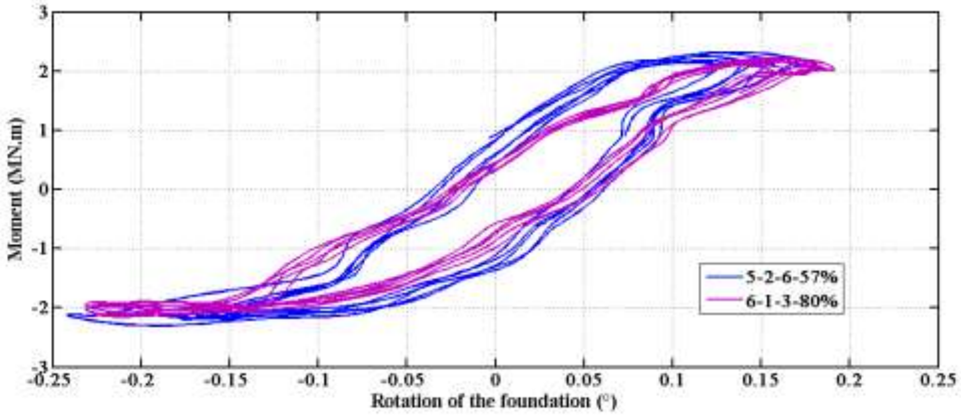

(b)

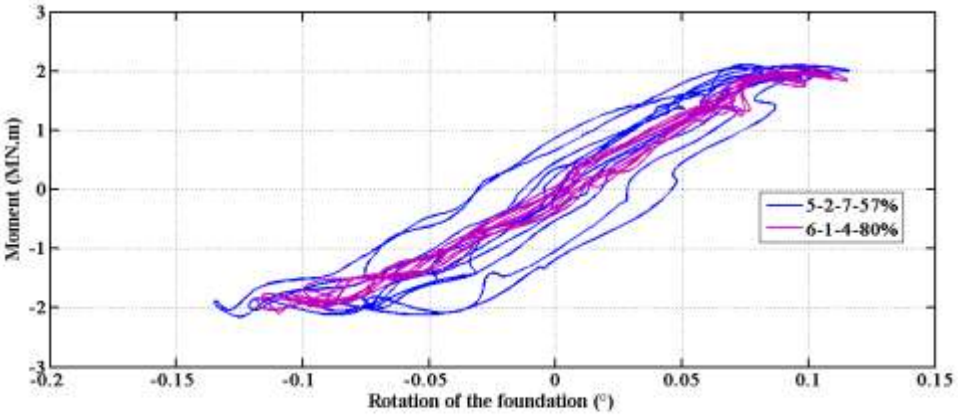

(c)

Figure 40: Relative Density Effects on Moment Rotation in the case of the 100kPa building (a) T1F1E1 input (b) T1F1E2 input (c) sine input.

In the case of the heavier building, 300 kPa, the decrease of the soil density induce an increase of soil-structure system damping especially in the case of the T1F1E1 and T1F1E2 inputs. In addition for the larger deformations (obtained for the T1F1E2 and sine inputs) larger rotation are obtained with the same moment value in the medium dense sand. This result is in accordance with the results obtained by UCAM on their structures. Considering the stiffness of the soil-structure system, such as previously mentioned the difference is in the order of the reproducibility discrepancy.

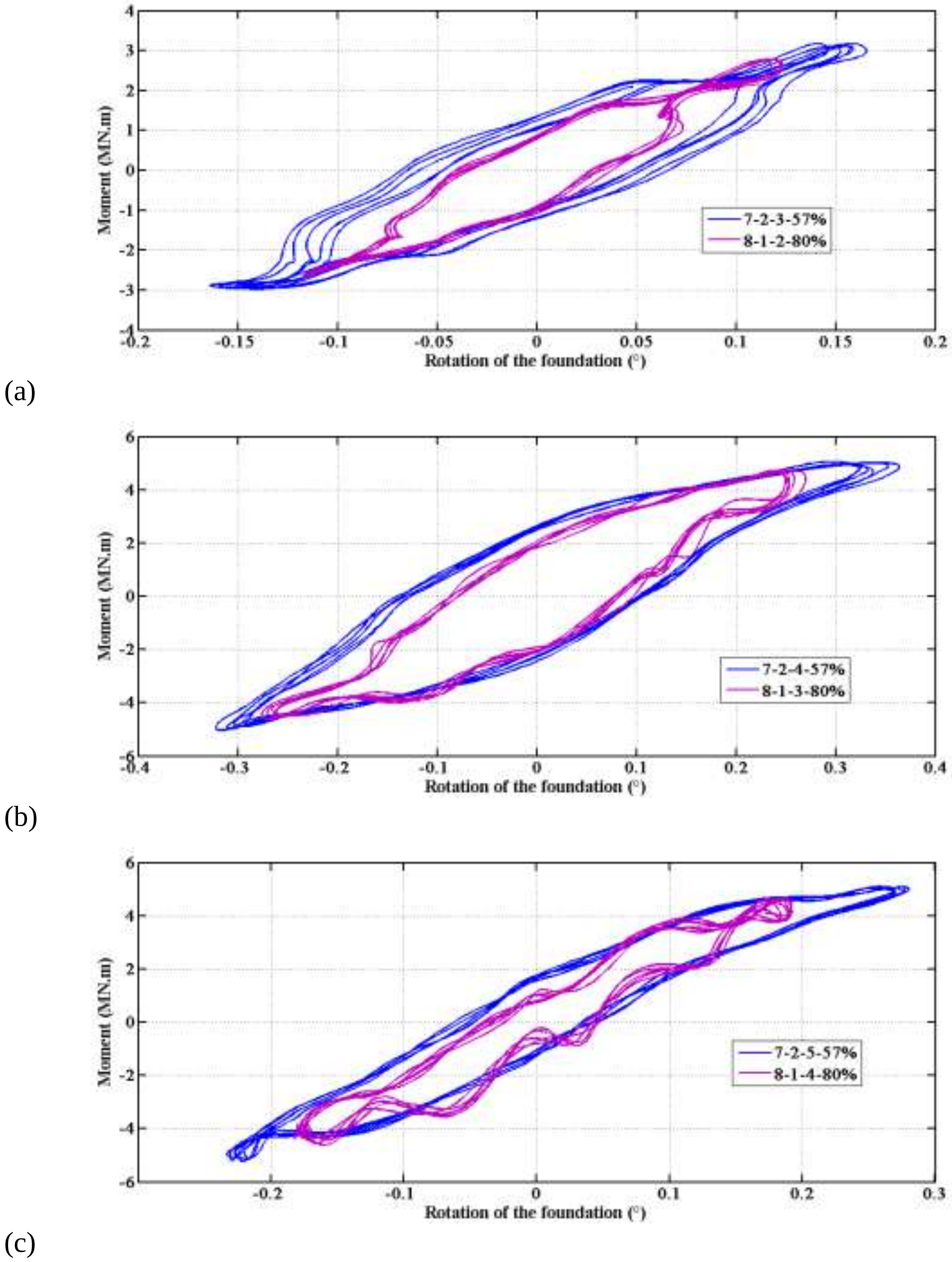

Figure 41: Relative Density Effects on Moment Rotation in the case of the 300kPa building (a) T1F1E1 input (b) T1F1E2 input (c) sine input.

Earthquake Frequency and Magnitude - UCAM

Increasing the magnitude of the earthquake could be expected to have a two fold effect. Primarily, the increased acceleration would be expected to result in larger accelerations in the structure and hence larger moments being applied through the footing onto the sand below. Consequently, it would be expected that larger rotations would occur when the larger moment is applied. Only a marginal increase in moment is observed in Figure 42 despite the peak rotations doubling. The larger ground accelerations do not appear to be transmitted in full through the soil-structure interface into the structure above. The increased rotations experienced could be a consequence of the larger earthquake displacements required during the stronger earthquake (given the fixed frequency). This would imply that the coupling of the structure with the soil is an important parameter in the analysis and that structural response may be dominated by the magnitude of the relative displacement between the ground and base of the structure, as opposed to simply the peak ground acceleration experienced. Despite only a small increase in moment, the increased rotation resulted in an increase in energy dissipation of over 200%. Ideally, the movement of the base of the structure relative to the sand below could be monitored and the variation with ground input acceleration observed. This is not possible with the data from the Phase I tests; however future particle image velocimetry analysis will allow any relative movements to be observed.

During Test CH04 two sine-sweep earthquakes were fired. One had significantly stronger amplitude than the other, with peak input accelerations of 16.8g and 24.1g. As discussed previously, the sine-sweep earthquake allows the system to be excited at every frequency from 60 Hz to 0 Hz. This allows the natural frequency of the system to be determined according to the input frequency at which the peak response of the superstructure occurs. The structures have a fixed base natural frequency of 50 Hz. During the small earthquake the natural frequency of the system was 42 Hz and this was further reduced to 38Hz during the large earthquake. This change in natural frequency is a consequence of the larger amounts of shear modulus degradation occurring in the soil during the stronger earthquake. This results in a softer, less stiff soil and hence the reduction in the natural period of the system observed in the results.

It has already been observed that the frequency of the earthquake affects the frequency at which the superstructures of the models vibrate. However, the frequency effect on the overall structure can be explored further through the moment rotation loops shown in Figure 42. Two earthquakes were fired during Test CH04 with similar acceleration magnitude but varying frequency. The 50 Hz earthquake was above the natural frequency of the structure-soil system but the 40 Hz earthquake was just below the natural frequency. As would be expected in any case where a system is excited closer to its natural frequency, substantially more response is observed with the lower frequency earthquake. The resulting rotations from the 40Hz earthquake were over three times those experienced during the 50 Hz earthquake. The sensitivity to frequency is not surprising but is rather alarming. When a building is being designed, the natural frequency of the structure may be evaluated without consideration of interaction effects with the ground below. Without a coupled design procedure that incorporates the soil-structure interaction effects, the true frequency at which the system is most volatile will not be known. When the moment-rotation loops from all cycles of the earthquake are plotted, the energy dissipated by the lower frequency earthquake (i.e. the area within the loops) is almost twice that of the 50Hz earthquake. These results may exaggerate the true problem as no real earthquake will be at a single frequency like in these experiments.

Another variation between the two frequency moment-rotation loops in Figure 42 is the apparent change in small strain stiffness between the two earthquakes. It would seem the higher frequency earthquake resulted in a higher stiffness between the footing and the soil. The larger peak rotations that occur during the lower frequency earthquake contribute to the strain softening of the soil within the soil-structure interface. Consequently this results in a less stiff response as the structure rotates through the zero rotation location as observed in the results.

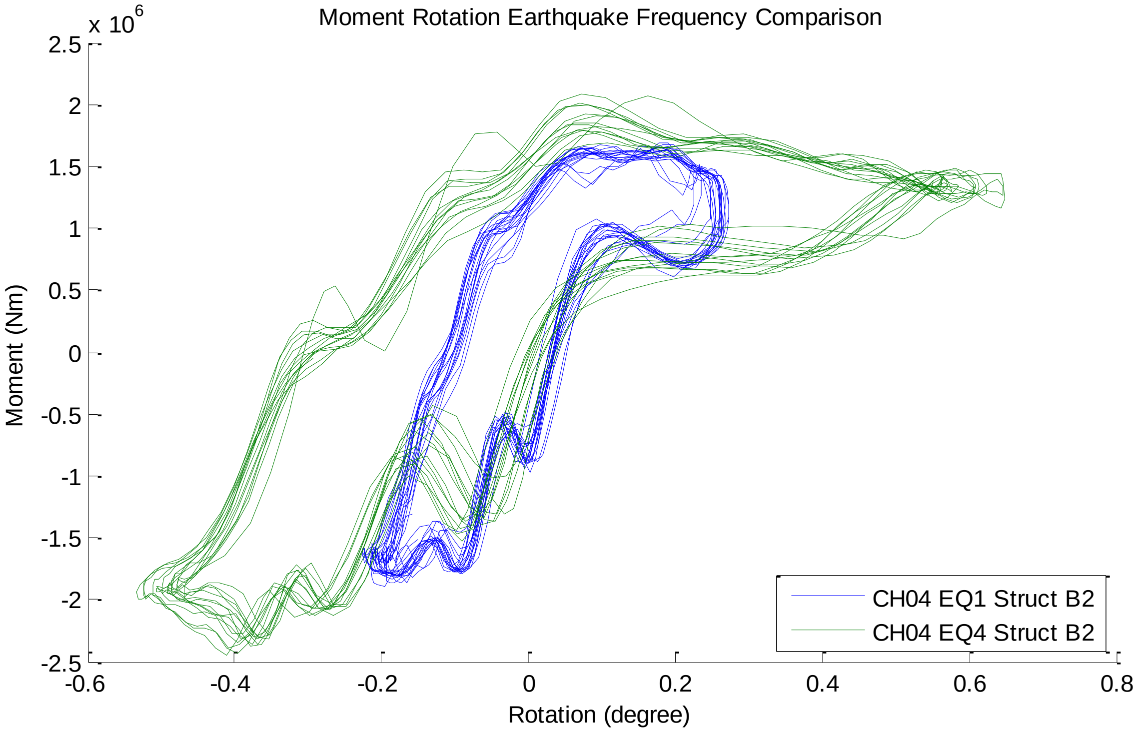

Figure 42: Earthquake Frequency Effect on Moment-Rotation Loops (CH04 EQ1 & EQ4 Struct B2)

Earthquake Frequency and Magnitude – IFSTTAR

The effect of the input on the moment rotation-loops is for each building (100 and 300 kPa) and each soil density (57 and 80%) on the Figures 43 to 46.

The effect of the earthquake frequency and magnitude is none negligible for both buildings and both soil density. In all the configurations the maximum rotation and moment obtained with T1F1E1 (Ai= 1.087m/s) are largely lower than that obtained with the T1F1E2 input (Ai=5.088m/s).

This result is in accordance with the two fold effects cited by UCAM. However such as noticed by UCAM the increase of the maximum rotation compared to that of the maximum moment is larger. It can be noticed that uplifting illustrating by an increase of the rotation at a constant level of moment appears only in the case of the lighter building.

Moreover another interesting results is that when a sine input is applied the maximum moment is almost the same as for the T1F1E2 input whereas the induce rotation is smaller. It indicate that in the case of the sine the soil-building system has a stiffer behaviour for the same level of moment inducing the the frequency also play a key role in the soil structure interaction.

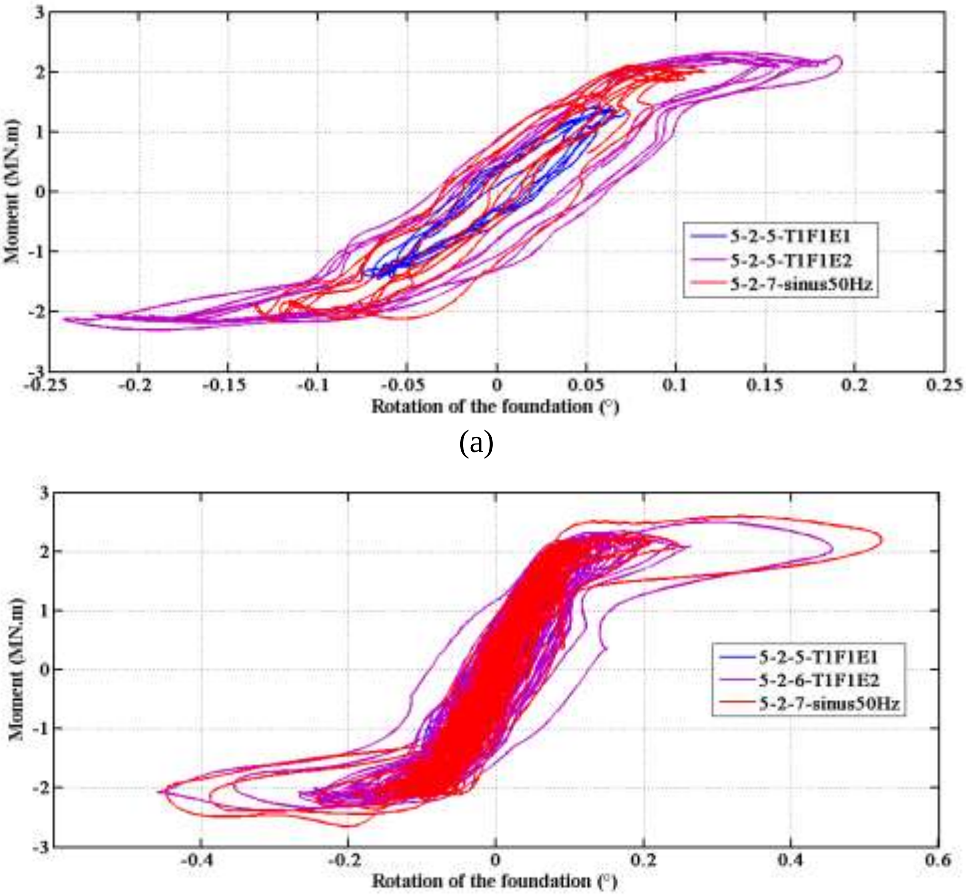

(a)

(b)

Figure 43: 100kPa building – Id=57% - Input effect on the on the Moment-Rotation Loops (a) selected loops (constant PGA level) and (b) all the recorded signal.

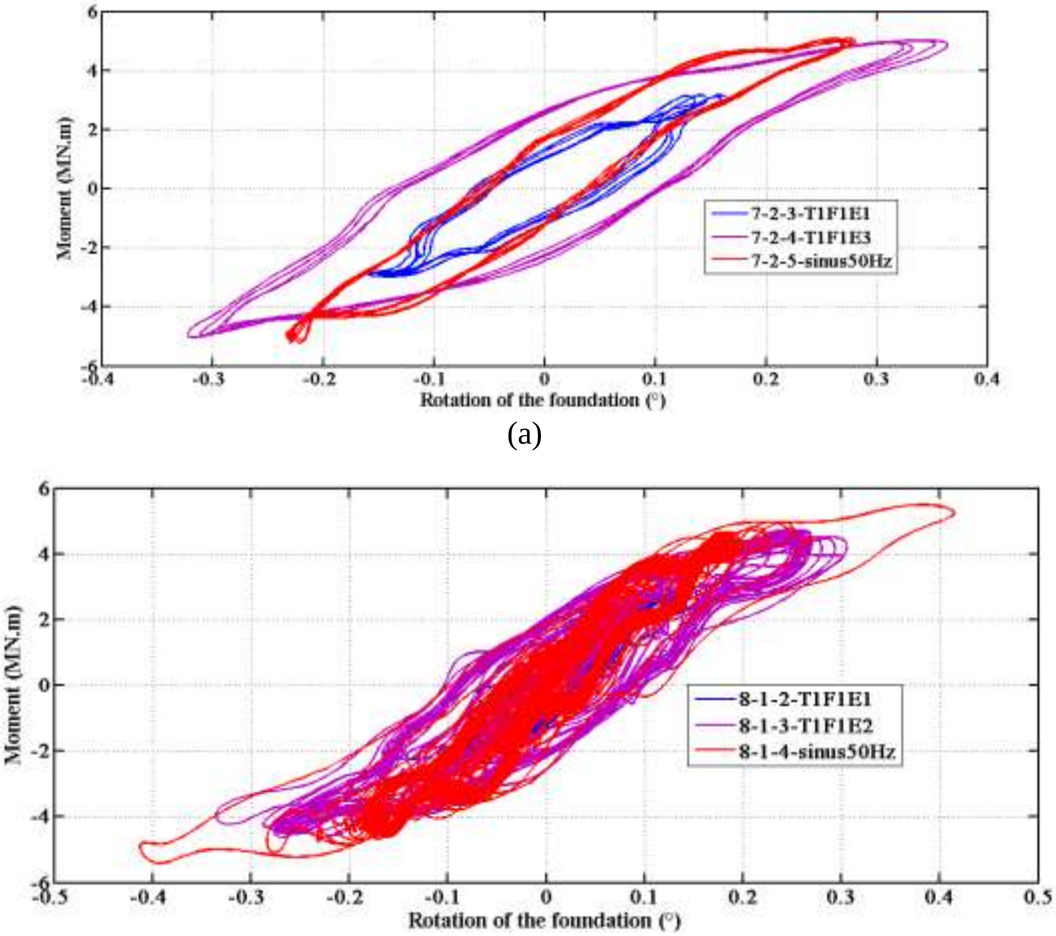

(a)

(b)

Figure 44: 300kPa building – Id=57% - Input effect on the on the Moment-Rotation Loops (a) selected loops (constant PGA level) and (b) all the recorded signal.

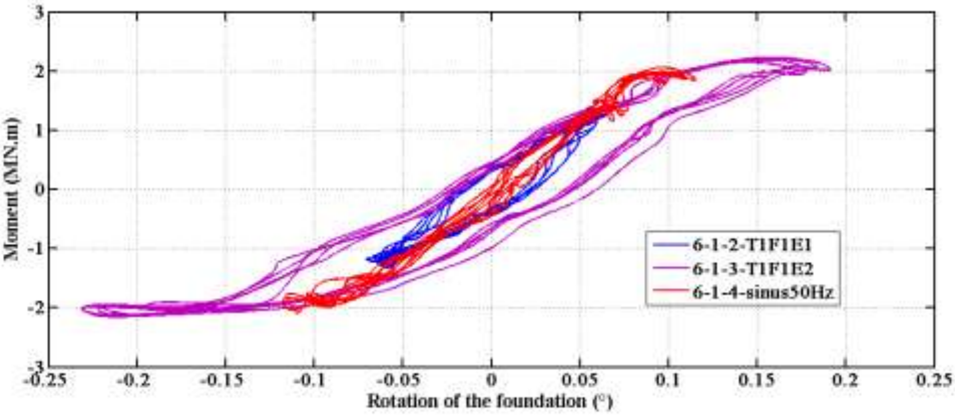

(a)

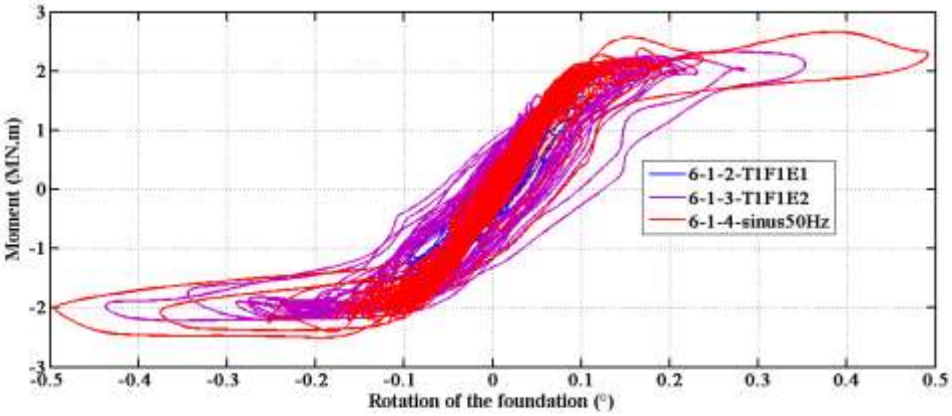

(b)

Figure 45: 100kPa building – Id=80% - Input effect on the on the Moment-Rotation Loops (a) selected loops (constant PGA level) and (b) all the recorded signal.

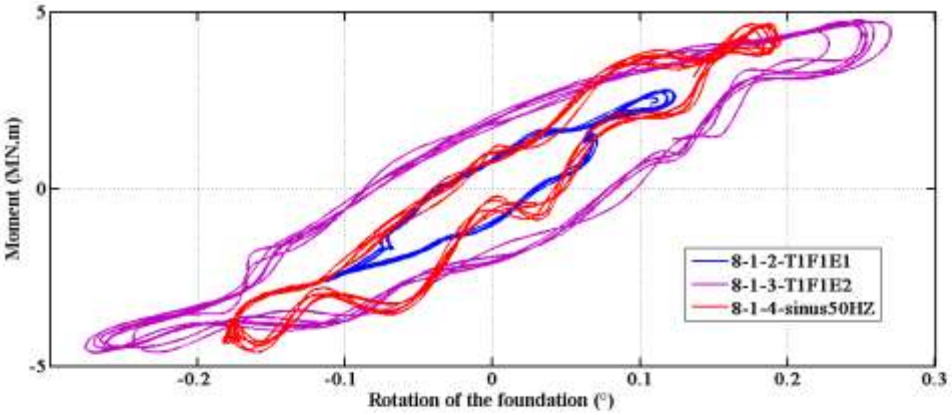

(a)

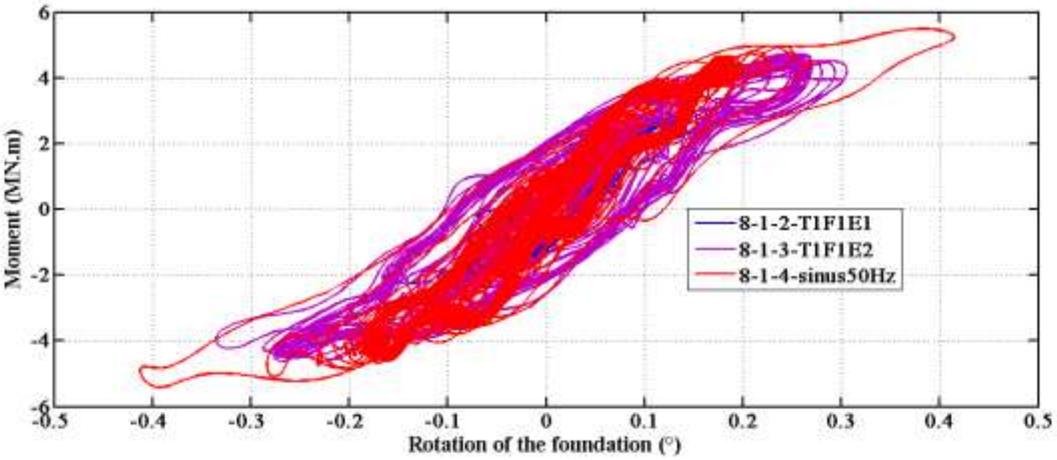

(b)

Figure 46: 300 kPa building – Id=80% - Input effect on the on the Moment-Rotation Loops (a) selected loops (constant PGA level) and (b) all the recorded signal.

Bearing Pressure-UCAM

It would be expected that increasing the bearing pressure of the footing would result in larger settlements occurring. Figure 47 proves this to be true. However, the difference between the settlements of the two structures is only 6mm (prototype scale). The larger structure, with twice the bearing pressure, experienced 30% more settlement compared to the lighter structure. However, this data is for a dense model. For a similar earthquake on loose sand (CH01 EQ2), the large structure settled by 250% of the settlement of the small structure. This highlights, as discussed previously, the significant impact of relative density on structural settlement. It can also be concluded that bearing pressure has a more significant impact on settlement rates at lower densities than at higher densities.

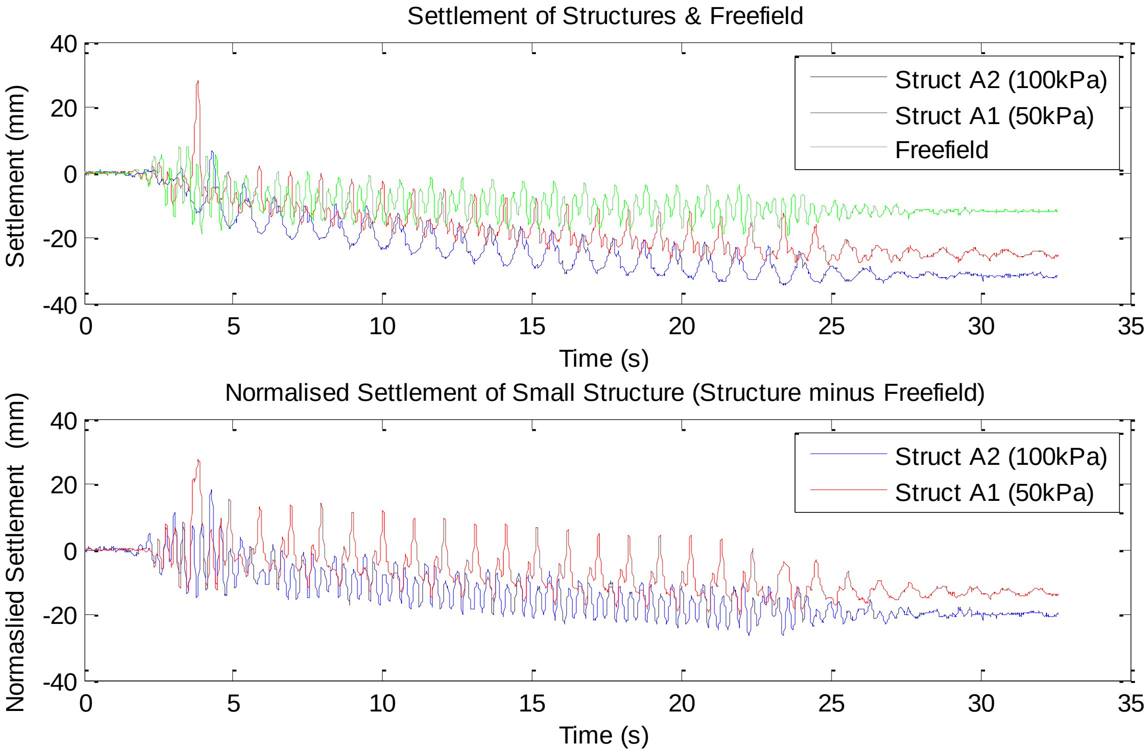

Figure 47: Bearing Pressure Effect on Settlement (CH02 EQ2)

Figure 48 shows the moment rotation loops for the two Type B structures during EQ2 of Test CH03. Naturally, the moment applied by the smaller footing is lower than that for the larger footing. However, the maximum angle of rotation is identical for both structures. The area within the entire set of moment-rotation loops for the large structure is twice the area contained within the loops for the small structure. The larger structure will always dissipate more energy as being heavier it will have more energy to dissipate in the first place. It is advantageous therefore to calculate the dimensionless damping factor, Equation 1, as was proposed by Hardin 1972. The dimensionless damping factor normalises the data by the magnitude of the maximum moment and rotation experienced, and hence allows a better comparison to be made between the energy dissipation of the two footings.

$$\mathbf{D = A_L / 4\pi A_T} \qquad \text{Equation 1}$$

Due to the unsymmetrical nature of the moment-rotation loops in Figure 48, the area of the rectangle that encapsulates the entirety of the moment rotation loops will be used as opposed to the area of the triangle formed between the origin and the loops apex. Consequently, the four is removed from the bottom of Equation 1 in the calculation. In addition, as opposed to using the total dissipated energy values quoted above, the loop area used is the value obtained from the average of the plotted loops only. Making these modifications results in a dimensionless damping factor value for the large structure of 0.0682 and for the small structure of 0.0564. The small structure subjects the ground below it to a lower confining stress than the large structure. This results in a lower stiffness and hence it is ‘easier’ for the foundation to rotate and thus less work is done in the process of it rotating. Therefore, the motion is less damped and less energy is dissipated, as seen in the dimensionless damping factors calculated.

The other feature of note in Figure 48 is the stiffer response of the larger structure at low angles of rotation, i.e. low strains. This comparatively stiffer response is due to two factors. Primarily, as discussed earlier, the larger footing subjects the sand below it to a greater confining stress compared to the small structure. This results in an increased stiffness. Secondly, it is likely densification will occur in the sand under the larger structure at a higher rate than under the smaller structure. As the ground densifies it will stiffen and hence a larger moment will be required to obtain the same amount of rotation of the foundation. If this is true, then as time passes and the small structure densifies the sand below it further, the small structure’s response at low strains should stiffen slightly. This is indeed observed when examining the moment rotation loops from the last few cycles of the shaking. The stiffness’s do not become identical however the small structure does experience an increasing small strain stiff response as time passes. It would not be expected that the stiffness’s would be identical due to the fundamental differences in confining stress’s.

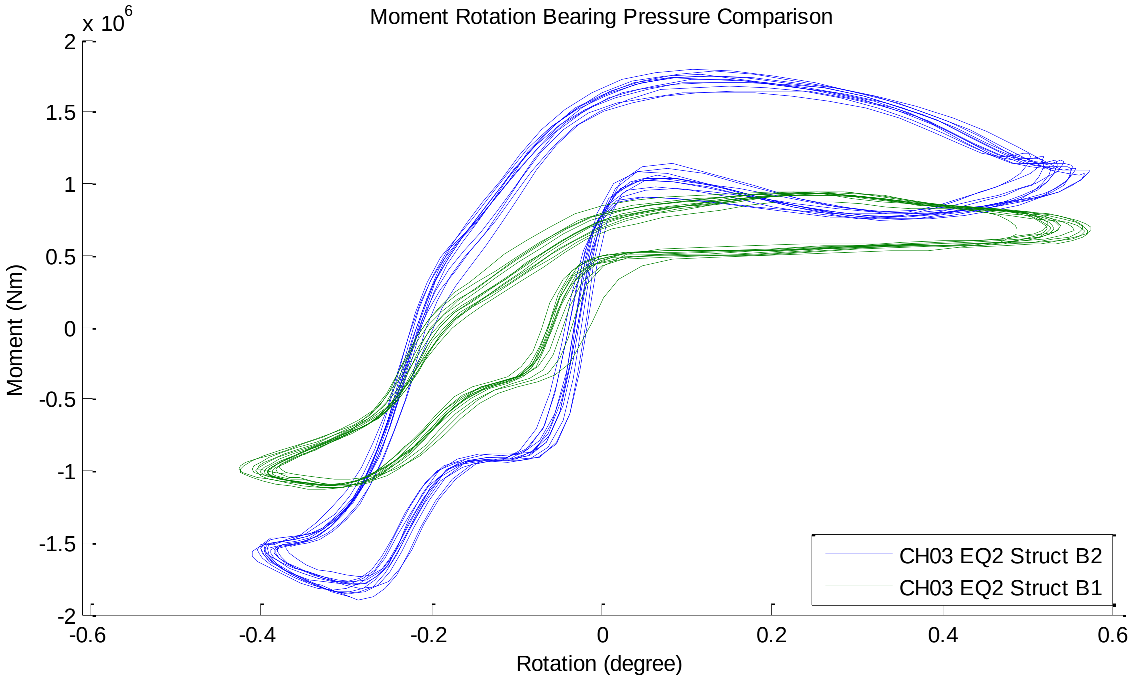

Figure 48: Bearing Pressure Effect on Moment-Rotation Loops (CH03 EQ2)

Bearing Pressure-IFSTTAR

The effect of the static bearing pressure applied by the building is analysed for the two soil densities and for the different inputs (T1F1E1, T1F1E2 and sinus). The results are presented in the Figures 49 to 51.

The effect of the static bearing pressure applied by the building is none negligible on the moment-rotation loops. For all the inputs and both soil density the maximum moment obtained with the heavier building is higher than that obtain with the lighter building.

For small rotation values, in the case of the medium dense sand, the variation of the stiffness of the soil-building with the type of building is not significant. However at larger rotation values and for the larger inputs, T1F1E2 and sine, rotation –moment loops highlight an uplift of the lighter building.

In the case of the dense sand, contrary to the lighter, the static bearing pressure of the building increases the stiffness of the soil-building system at low rotation value. This point remains valuable for all the type of input. Thus the effect of the bearing pressure apply by the superstructure seems to be influenced by the soil density. The effect on the stiffness at low level of rotation seems to be higher when the sand is denser.

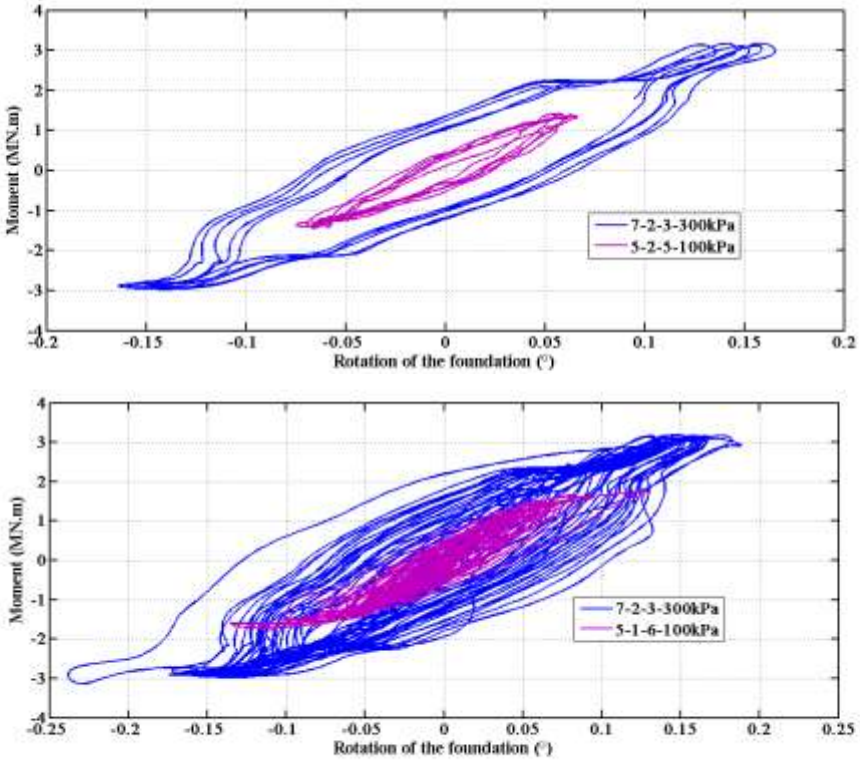

(a)

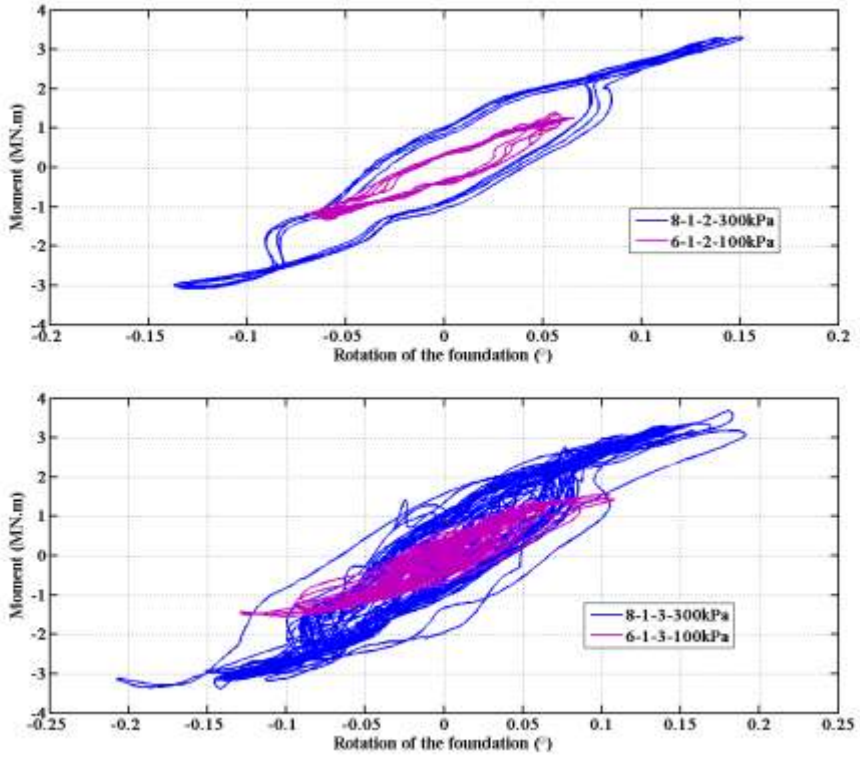

(b)

Figure 49: T1F1E1 - Bearing Pressure Effect on Moment-Rotation Loops (a) Id=57% selected loops (full amplitude) and all the recorded data (b) Id=80% selected loops (full amplitude) and all the recorded data

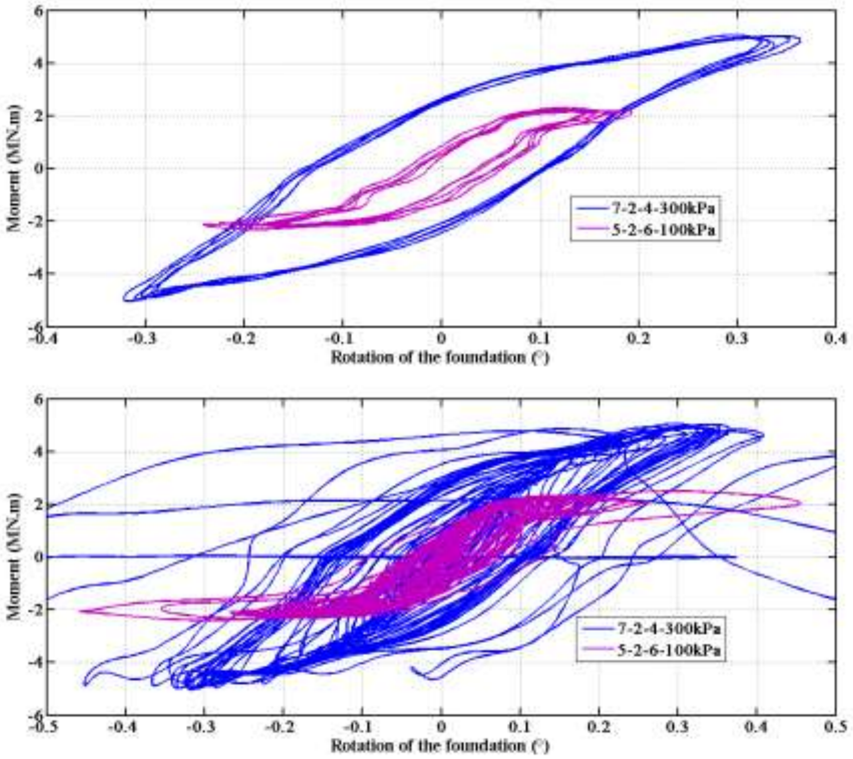

(a)

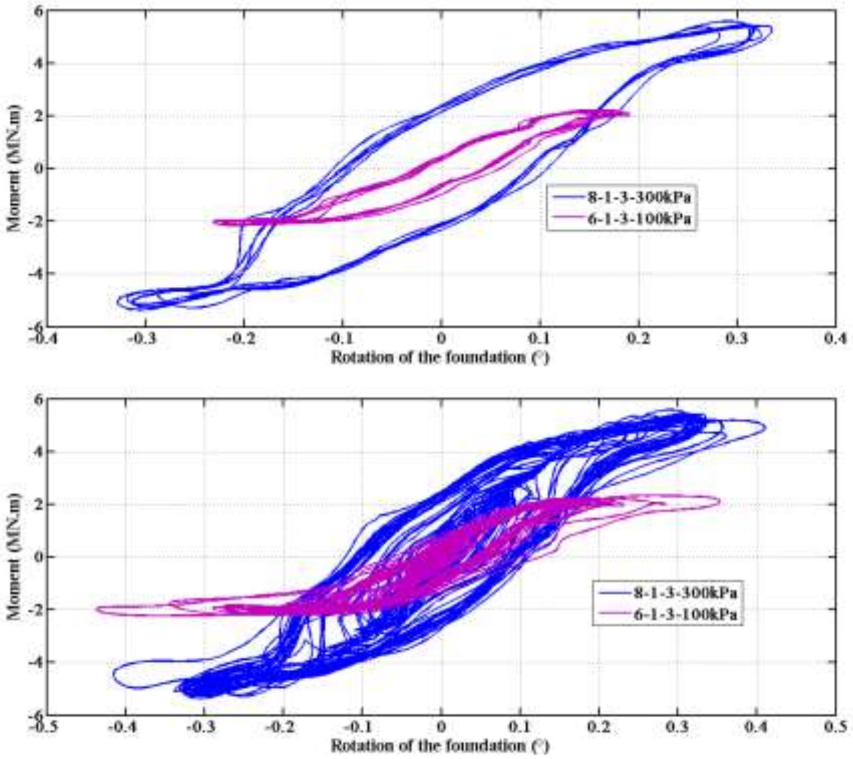

(b)

Figure 50: T1F1E2 - Bearing Pressure Effect on Moment-Rotation Loops (a) Id=57% selected loops (full amplitude) and all the recorded data (b) Id=80% selected loops (full amplitude) and all the recorded data

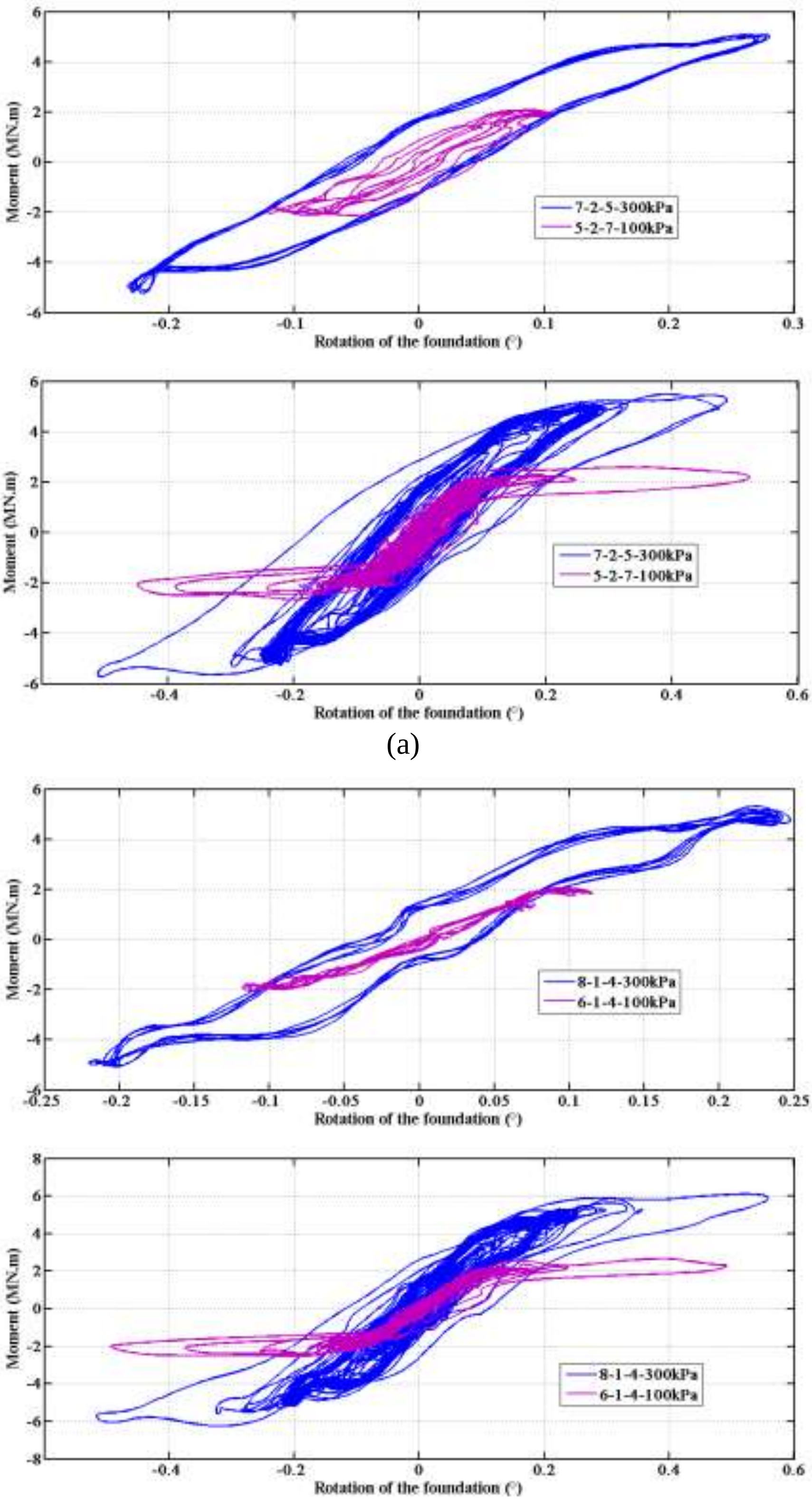

(a)

(b)

Figure 51: Sine - Bearing Pressure Effect on Moment-Rotation Loops (a) Id=57% selected loops (full amplitude) and all the recorded data (b) Id=80% selected loops (full amplitude) and all the recorded data

Particle Image Velocimetry (PIV)

Despite a full analysis having yet to be completed on the data from the PIV tests; it is still possible to present some preliminary results. The most common use of PIV in geotechnical testing is to examine how the soil deforms while performing a certain test, e.g. tunnelling, excavation, dynamic shaking, etc.

Figure 52 shows the soil deformation during Test CH10 Flight 1 EQ2 which used structure D2a. Significant deformation occurs during the quarter cycles immediately after a change in direction. The major impact of the deformation mechanism is only experienced to a depth of about half the footing width. Once the full analysis is completed, information on deformation mechanism depth will be valuable for ensuring ground investigation works and subsequent remediation works are conducted to the appropriate depth under shallow foundations in seismically active areas.

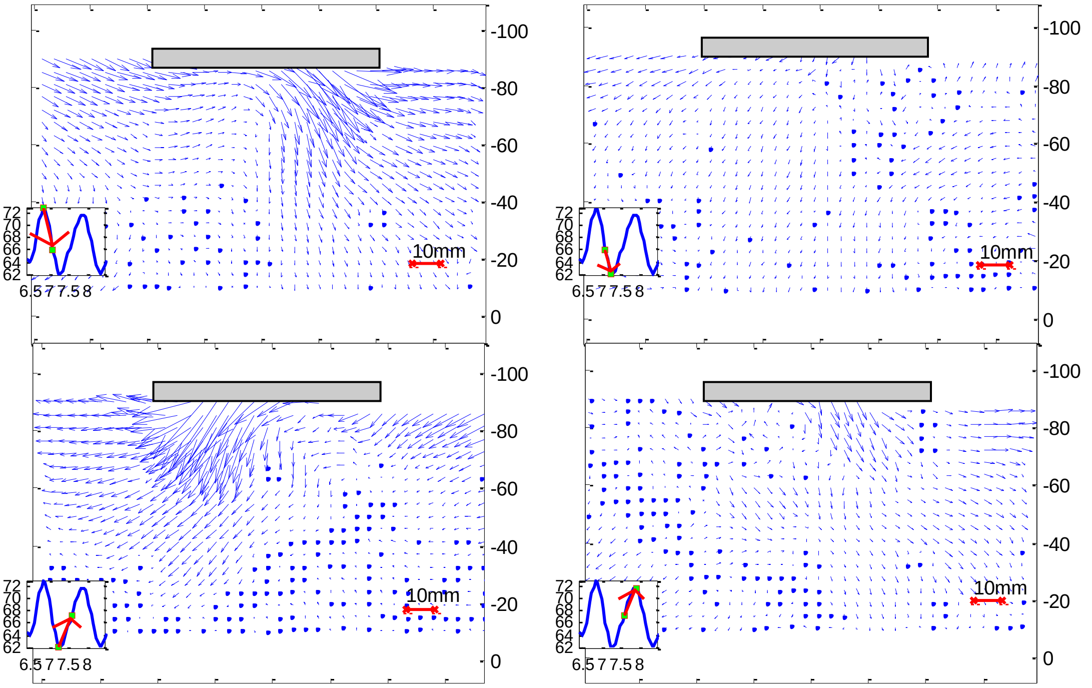

Figure 52: Soil deformation through one cycle of CH10 Flight 1 EQ2

Using the same Geo-PIV technique it is also possible to track points between images. This was utilised to track the movement of the model structures during the dynamic shaking. Being able to capture this movement allows accurate moment-rotation and settlement-rotation plots to be produced.

Figure 53 shows the settlement rotation for structures C1 and C2 sited on the same density of sand and subjected to the same earthquake. The stiff C2 structure experiences significantly more rotation than the flexible C1 structure. This is due to the C1 structure being able to dissipate energy internally whereas the C2 structure dissipates the majority of the dynamic energy through the soil-structure interface and hence experiences significantly more rocking. The marginal increase in settlement experienced by the C2 structure is likely due to small variations in the true relative densities of the models.

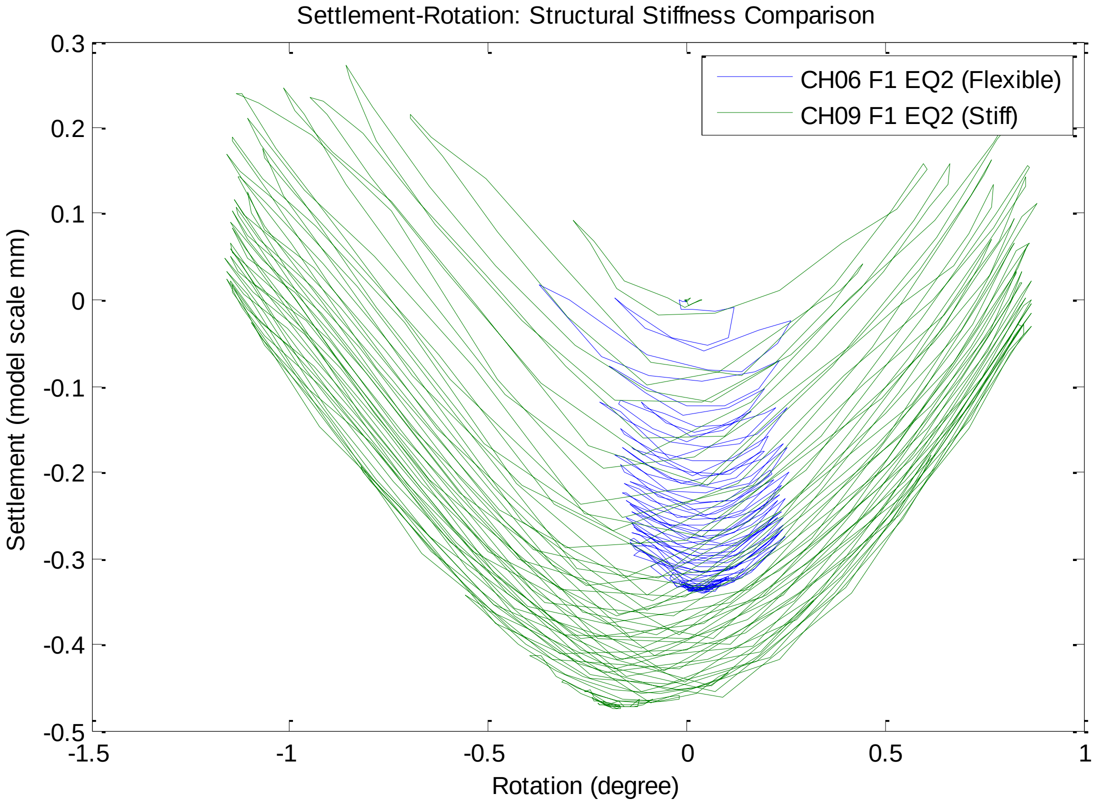

Figure 53: Settlement-rotation curves: CH06 F1 EQ2 & CH09 F1 EQ2

Another aspect that can be investigated with settlement-rotation curves is the impact of relative density. Figure 54 shows the settlement-rotation curves for two identical earthquakes with identical structures, however one was on a loose (50%) model and one was on a dense (80%) model. As discussed earlier with respect to the moment-rotation loops, the structure on the loose sand densifies the sand beneath it as it settles. After about four cycles the sand beneath the structure has densified to a state whereby the amount of settlement per rocking cycle decreases significantly. The structure on the dense soil on the other hand does not induce much settlement and instead experiences larger rotations as a means of dissipating the seismic energy. One aspect of this particular settlement-rotation comparison that requires further investigation is the decreasing magnitude in rotation experienced by the structure on the loose sand once the initial large settlement rate has passed. Further investigation of the concurrent soil deformations should allow this phenomenon to be explained.

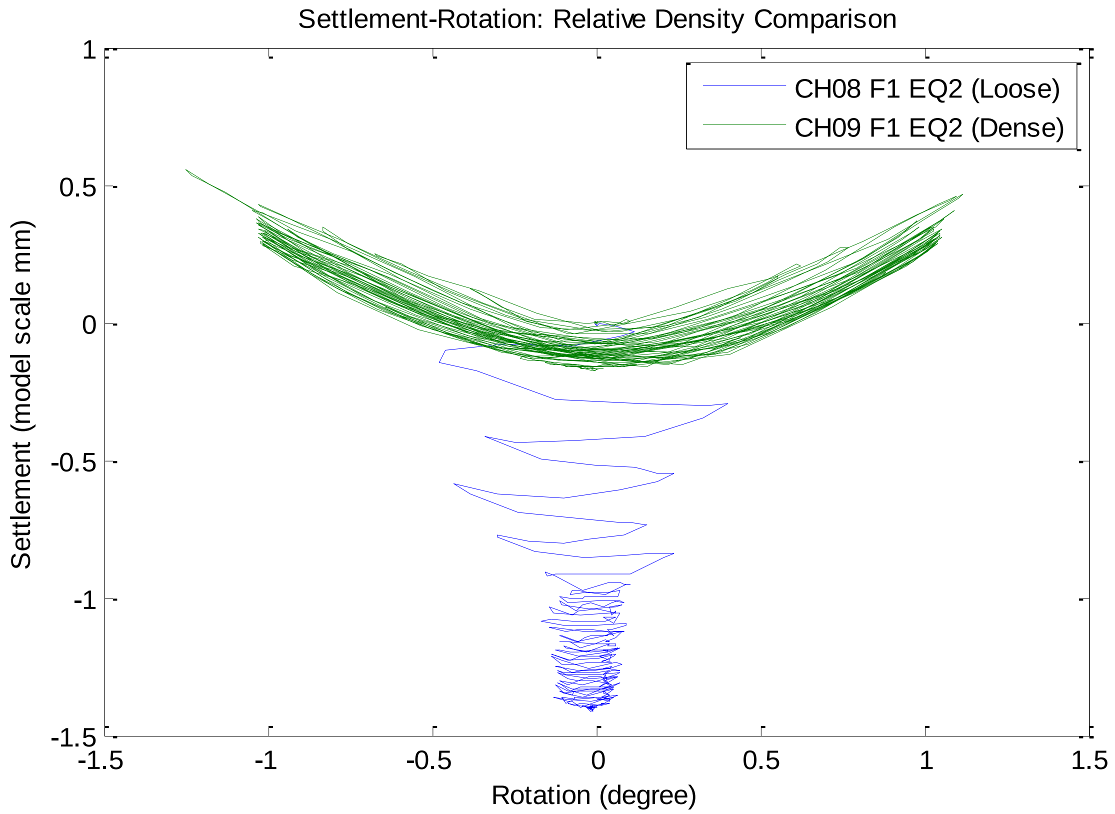

Figure 54: Settlement-rotation curves: CH08 F1 EQ2 & CH09 F1 EQ2

Summary

In this work package (JRA3.2) extensive centrifuge modelling was carried out at both UCAM and IFSTTAR to investigate the dynamic soil-structure interaction of single degree of freedom structures. The following parameters were considered:

- Structural stiffness and mass leading to structures of different natural frequencies
- Height of centre of gravity
- Bearing pressure exerted by the structure on the foundation soil
- Relative density of the foundation soil
- Earthquake intensity and frequency content including both sinusoidal shaking and more realistic earthquakes

Following from Phase I testing it was found that a good agreement was seen between the results of nominally identical centrifuge models tested at the two centres. This enables us to compare with confidence the results from Phase II and III at the two centres.

It was observed that increasing structural stiffness led to increased displacements of the structural base. Increasing the height of the centre of gravity led to a less stable structure that oscillated more during the earthquake loading.

Structures that exerted larger bearing pressure suffered more settlement during the earthquake loading.

Relative density of soil was found to be an important parameter. Increasing relative density led to a decrease in settlements but an increase in the rotation amplitude of foundation. This was established by constructing settlement-rotation curves based on PIV image analyses.

It was found that earthquake intensity did not significantly affect the peak rotation of the foundation. It was found that there is a threshold acceleration amplitude that is required to cause lift-off of the foundation from the soil. Earthquake driving frequencies close to the natural frequency of the soil-structure system led to increased deformations in the soil and the structure. The natural frequency of the soil-structure system is different from that of the fixed base structure. This confirms that the stiffness of the foundation soil plays an important role in the dynamic response of the overall soil-structure system.

While these are preliminary observations, the data obtained in these series of centrifuge tests will be further analysed through the remainder of the SERIES project and disseminated through the final project workshop in 2013 at ISPRA along with publications in top ranked journals.

References

Brennan, A.J. and Madabhushi, S.P.G., (2002), Design and Performance of a new deep model container for dynamic centrifuge testing, Proc. International Conference on Physical Modelling in Geotechnics, St John's, Newfoundland, Canada, July, pp 183-188.

Chian, S.C., Stringer, M.E. and Madabhushi, S.P.G., (2010), Use of Automatic Sand Pourer for Loose Sand Models, Proc. 7th International Conference on Physical Modelling in Geotechnics, Zurich, Switzerland.

Cilingir, U. and Madabhushi, S.P.G., (2010), Particle Image Velocimetry Analysis in Dynamic Centrifuge Tests, Proc. 7th International Conference on Physical Modelling in Geotechnics, Zurich, Switzerland.

Cilingir, U. and Madabhushi, S.P.G., (2011), A model study on the effects of input motion on the seismic behaviour of tunnels, Journal of Soil Dynamics and Earthquake Engineering, Vol. 31, pp. 452-462.

Escoffier, S., (2008), Conteneur ESB, LCPC Internal report no: 2007-1-13-1/1-a, 106p.

Flavigny,E., Desrues, J. and Palayer,B., (1990), le sable d'hostun, Geotechnique, Vol.53, pp 67–70.

Hardin, B.O. and Drnevich, V.P., (1972), Shear modulus and damping in soils: Measurement and parameter effects. Soils Mechanics and Foundations Division, 98(SM6), pp 603–624.

Madabhushi, S.P.G., Schofield, A.N. & Lesley, S.,(1998), A new stored angular momentum (SAM) based earthquake actuator. Proc. Of Centrifuge '98, Balkema, Rotterdam, 111-116.

Madabhushi, S.P.G., Houghton, N.E. and Haigh, S.K., (2006), A new automatic sand pourer for model preparation at University of Cambridge, Proc. 6th International Conference on Physical Modelling in Geotechnics, Hong Kong.

Schofield, A.N., (1980), Cambridge geotechnical centrifuge operations, Geotechnique, Vol.30(3), pp. 227-268.

Schofield, A.N., (1981), Dynamic and earthquake geotechnical centrifuge modelling, Proc. Int. Conf. on Recent Advances in Geotechnical Earthquake Engineering and Soil Dynamics, University of Missouri-Rolla, MO, USA, pp 1081-1100.

Steedman, R.S. and Madabhushi, S.P.G., (1991), Wave propagation in sand medium, Proc. of Fourth Intl. conference on Seismic Zonation, Stanford University, Palo Alto, California, USA.

Stringer, M.E., Heron, C.M. & Madabhushi S.P.G, (2010), Experience using MEMS-based accelerometers in dynamic testing, Proc. Physical Modelling in Geotechnics ICPMG 2010, pp 389-394.

White D.J, (2002), GeoPIV: Particle Image Velocimetry (PIV) software for use in geotechnical testing. University of Cambridge Department of Engineering, Technical Report No. CUED/D-SOILS/TR322.

Zhao, Y., Gafar, K, Thusyanthan, N.I., Knappett, J.A., Mohamed, H., Deeks, A. and Madabhushi, S.P.G., (2006), Calibration and Use of a New CNC Automatic Sand Pourer, Proc. International Conference on Physical Modelling in Geotechnics Centrifuge’06, Hong Kong.